

Current and Future Rainfall-Driven Flood Risk From Hurricanes in Puerto Rico Under 1.5°C and 2°C Climate Change

Leanne Archer¹, Jeffrey Neal¹, Paul Bates¹, Emily Vosper¹, Dereka Carroll², Jeison Sosa³, Daniel Mitchell¹

¹School of Geographical Sciences, University of Bristol, Bristol, UK

²Department of Chemistry, Physics, and Atmospheric Sciences, Jackson State University, Jackson MS, United States

³Fathom, Bristol, UK

Correspondence to: Leanne Archer (leanne.archer@bristol.ac.uk)

Abstract

Flooding associated with Hurricane Maria in 2017 had devastating consequences for lives and livelihoods in Puerto Rico. Yet, an understanding of current and future flood risk in small islands like Puerto Rico is limited. Thus, efforts to build resilience to flooding associated with hurricanes remain constrained. Here, we take an event set of hurricane rainfall estimates from a synthetic hurricane rainfall simulator as the input to an event-based rainfall-driven flood inundation model using hydrodynamic code LISFLOOD-FP. Validation of our model against High Water Mark data for Hurricane Maria demonstrates the suitability of this model for estimating flood hazard in Puerto Rico. We produce event-based flood hazard and population exposure estimates for the present day, and the future under the 1.5°C and 2°C Paris Agreement goals. Population exposure to flooding from hurricane rainfall in Puerto Rico for the present day climate is approximately 8-10% of the current population for 5-year return period, with an increase in population exposure to flooding by 2-15% and 1-20% under 1.5°C and 2°C futures (5-year return period). This research demonstrates the significance of the 1.5°C Paris Agreement goal for Small Island Developing States, providing the first event-based estimates of flooding from hurricane rainfall under climate change in a small island.

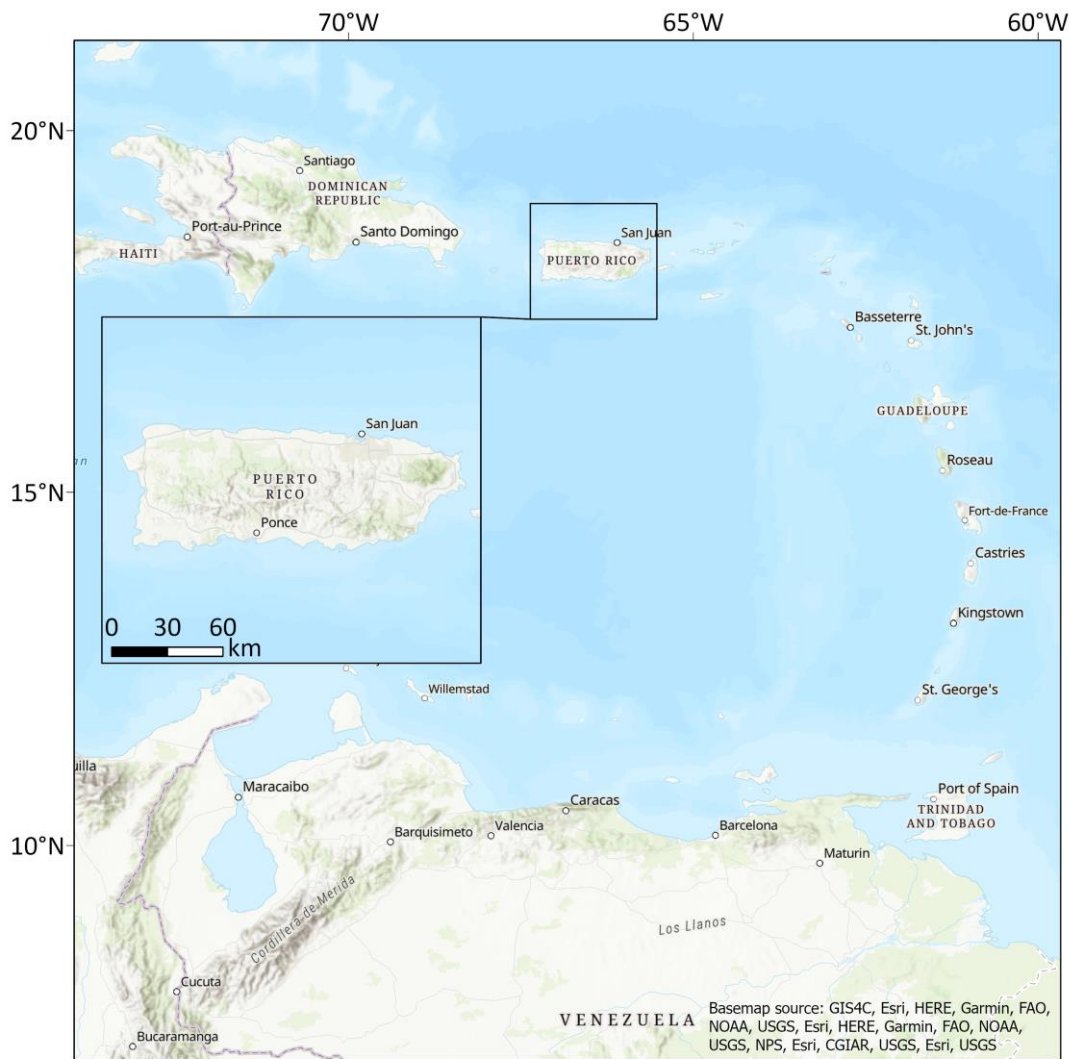
1 Introduction

Climate change is amplifying the probability of high intensity tropical cyclone events globally (Patricola and Wehner, 2018; Kossin et al., 2020; Mei and Xie, 2016; Knutson et al., 2020), compounding the rising social and economic costs associated with disasters due to increasing population and asset exposure (Jiménez Cisneros et al., 2014). The adoption of the Paris Agreement in 2015 aimed to limit global warming to well below 2°C above pre-industrial levels, and if possible to 1.5°C (United Nations Framework Convention on Climate Change, 2015). Following this, numerous studies have investigated how these global temperature changes could impact societies, ecosystems, and places (IPCC, 2018; Mitchell et al., 2016). Under the upper Paris Agreement goal of 2°C, there will likely be a higher proportion of tropical cyclones that become the most intense storms (i.e. Category 4 and 5 hurricanes), with an increase in precipitation intensity (Knutson et al., 2020). Whilst flooding accounts for the largest proportion of loss of life and economic damages from tropical cyclones (Rappaport, 2014; Czajkowski et al., 2017), there is a lack of literature exploring how flooding might be affected by changes in tropical cyclone characteristics under climate change. This is particularly pertinent for Small Island

39 Developing States where the difference between the 1.5°C and 2°C temperature goals may be critically
40 important (Hoegh-Guldberg et al., 2018).
41

42 Small Island Developing States (SIDS) are a group of small island nations and territories with an acute risk of
43 disasters and the impacts of climate change, who were an instrumental force in the implementation of the 1.5°C
44 goal in the Paris Agreement (Ourbak and Magnan, 2018). Considering risk as a function of hazard, exposure and
45 vulnerability (Terminology, 2019), high hazard frequency, high exposure in relation to size and underlying
46 vulnerabilities drive the risk of hydrometeorological disasters and climate change in SIDS (Nurse et al., 2014;
47 Mycoo et al., 2022). Climate change is likely to exacerbate current flood risk in SIDS (Joyette et al., 2014;
48 Thomas et al., 2017) based on projected changes in tropical cyclone precipitation (Vosper et al., 2020),
49 increased coastal storm surge heights (Knutson et al., 2020; Monioudi et al., 2018) and sea level rise (Storlazzi
50 et al., 2018; Nicholls et al., 2018; Rasmussen et al., 2018). Yet, very little island-scale quantitative assessment of
51 flood risk has been conducted in SIDS. This is largely due to the inadequacy of existing methods as well as
52 insufficient data resolution and quality suitable for the scale of small island modelling (typically <10,000km²)
53 (Thomas et al., 2019).
54

55 Recent work by Vosper et al., (2020) demonstrates that total rainfall associated with tropical cyclones (also
56 known as hurricanes) in the Caribbean will increase under both the 1.5°C and 2°C Paris Agreement goals in
57 comparison to the present day climate. They also estimate that a 100-year return period event similar to
58 Hurricane Maria in Puerto Rico would be twice as likely to occur under the 2°C scenario than the 1.5°C scenario
59 (Vosper et al., 2020). Puerto Rico is an unincorporated territory of the United States located in the Greater
60 Antilles islands of the Caribbean (see Figure 1). The urgent need to understand both current and future flood risk
61 was recently reinforced following Hurricane Maria in 2017, which made landfall as a high-end Category 4
62 hurricane, causing catastrophic wind and flood damage (Pasch et al., 2018). Hurricane Maria was the strongest
63 hurricane to hit Puerto Rico since Hurricane San Felipe II in 1928, resulting in at least 2975 deaths (Audi et al.,
64 2018). The estimated economic loss of US\$90 billion made it the third costliest disaster in US history (Pasch et
65 al., 2018). Despite the underlying structural failures and inadequate emergency response that also contributed to
66 the scale of the disaster in Puerto Rico (Towe et al., 2020; Rivera, 2020; Caban, 2019; Willison et al., 2019), the
67 volume and intensity of the rainfall associated with Hurricane Maria was unprecedented and exacerbated the
68 scale of the impact on communities on the island (Keellings and Hernández Ayala, 2019; Ramos-Scharrón and
69 Arima, 2019). Historically, hurricane rainfall has been the key cause of flooding in Puerto Rico (Hernández
70 Ayala et al., 2017; Smith et al., 2005). Consequently, it is pertinent that estimates of current and future rainfall-
71 driven flood risk associated with these hurricane rainfall events are developed to assist disaster risk management
72 in Puerto Rico. Yet, there are currently no complete estimates of flooding associated with Hurricane Maria, or
73 indeed for any other events in Puerto Rico. Dated FEMA flood zone maps do exist for larger river systems in
74 Puerto Rico, but these do not include pluvial flooding which is a key focus of this paper. They are therefore
75 likely to provide a considerable underestimate of risk (Wing et al., 2017).



76

77 **Figure 1 - Map showing the island of Puerto Rico within the Caribbean region.**

78

79 Tropical cyclones can generate pluvial, fluvial and coastal floods, all of which interact. Of these pluvial flooding
 80 is a comparatively lesser modelled phenomenon (Blanc et al., 2012; Rözer et al., 2019; Tanaka et al., 2020).

81 Pluvial flooding is defined here as ‘flooding resulting from rainfall-generated overland flow and ponding before
 82 the runoff enters any watercourse or drainage system, or cannot enter it because the network is full to capacity’
 83 (Falconer et al., 2009, p.199). There has been a historical split between the modelling and assessment of pluvial
 84 and fluvial – or river - flooding. However, in reality both of these inland flood types are in a continuum, and
 85 both driven by rainfall. Thus, the distinction between the two is unhelpful in many cases. This is particularly
 86 true in small islands where much of the inland flooding is primarily driven by heavy rainfall (Jetten, 2016;
 87 Burgess et al., 2015). Pluvial flooding is also a contested term, with some defining it as including small river
 88 channels (Wing et al., 2018), and other defining it as completely independent of rivers (Rosenzweig et al., 2018;
 89 Hankin et al., 2008). The rain on grid approach documented here therefore overcomes this pluvial/fluvial
 90 distinction by explicitly modelling both flood types and their interactions. Here we define the flooding modelled
 91 in this approach as ‘rainfall-driven flooding’.

92

93 Rainfall-driven flood events can often occur with a high frequency but low magnitude. This can lead to a
94 significant cumulative impact on a community's resilience over time which can undermine efforts to reach the
95 UN's Sustainable Development Goals (Moftakhari et al., 2017; Hamdan, 2015; United Nations Office for
96 Disaster Risk Reduction, 2019). However, most studies investigating flooding under climate change focus on
97 changes in the 100-year flood extent because this is often used as a design standard (Hirabayashi et al., 2013;
98 Arnell and Gosling, 2016; Lehner et al., 2006). This means the critical understanding of how smaller, more
99 frequent events might vary under climate change remains, which have a crucial importance for improving the
100 resilience-building and climate change adaptation needed in local communities (Moftakhari et al., 2017). This
101 paper aims to address this gap by investigating how changing hurricane rainfall characteristics influence
102 rainfall-driven flood risk estimates in Small Island Developing State Puerto Rico, with an emphasis on
103 understanding changes in lower magnitude, higher frequency events (<30-year return period).

104

105 Currently, the predominant method for understanding changes in flooding under climate change in small islands
106 uses changes in precipitation as a proxy for changes in flood hazard, leading to uncertainty in flood hazard
107 changes under climate change (Seneviratne et al., 2021; Ranasinghe et al., 2021). Examples of pluvial hydraulic
108 flood modelling in small islands have previously relied on spatially uniform rainfall estimates derived from
109 historical data for a set of design return period events (World Bank, 2015; Pratomo et al., 2016; Lumbroso et al.,
110 2011). This approach takes a set of rainfall intensity estimates for a given duration and return period, often
111 derived from an Intensity-Duration-Frequency (IDF) curve using historical rainfall data. Rainfall is typically
112 applied uniformly across a model domain to produce design event flood extents (World Bank, 2015). Yet, this
113 approach does not necessarily represent flooding at a particular return period, as a flood is a signature of the
114 rainfall, the topography and the topology of a catchment (Guerreiro et al., 2017; Skougaard Kaspersen et al.,
115 2017). More recently, studies have highlighted the importance of representing rainfall spatially and temporally
116 for a more realistic representation of flooding (Aldridge et al., 2020; Bernet et al., 2019; Guerreiro et al., 2017;
117 Schaller et al., 2020). One way of incorporating these features is through an 'event set approach', which
118 involves utilizing an event set of synthetic rainfall events (Nuswantoro et al., 2016; Tanaka et al., 2020).
119 Nonetheless, data such as this are still limited or non-existent – particularly in small islands – and thus the
120 aforementioned traditional approach has until now the only way to represent flood hazards for small islands.
121 Climate change is often assessed by applying an uplift factor to account for changes in rainfall associated with
122 climate change projections (Sayers et al., 2020). However, this approach also fails to account for non-stationary
123 effects of climate change on flooding, including changes to the different spatial and temporal characteristics of
124 rainfall that are important for flood generation (Rosenzweig et al., 2018).

125

126 This paper details the first example of an event-based assessment of flood hazard in a small island under current
127 and future climate change. We utilise a synthetic hurricane rainfall data set (Vosper et al., 2020) as the input to
128 an event-based rainfall-driven hydrodynamic flood model of Puerto Rico. We model rainfall-driven flood
129 hazard and population exposure at the island scale in Puerto Rico (9100km²), at 20m resolution under present
130 day, 1.5°C and 2°C climate change. As part of this work, we also include novel methodological developments,
131 including the representation of rainfall and river channels in the model. The model is validated against flood
132 hazard simulations using two estimates of Hurricane Maria observed rainfall (IMERG and NCEP Stage IV) and

133 High Water Mark data collected from the event. To our knowledge, these are the first published estimates of
134 rainfall-driven flooding from Hurricane Maria. This work thus demonstrates a step-change in the capacity to
135 estimate flood hazard in a small island, superseding the information available using the traditional approaches.
136 Within this, two key questions will be investigated:

- 137 1) What is the current rainfall-driven flood hazard and population exposure associated with hurricanes in
138 Puerto Rico?
- 139 2) How does population exposure to flooding change from present day under 1.5°C and 2°C climate
140 change scenarios?

141 **2 Methods**

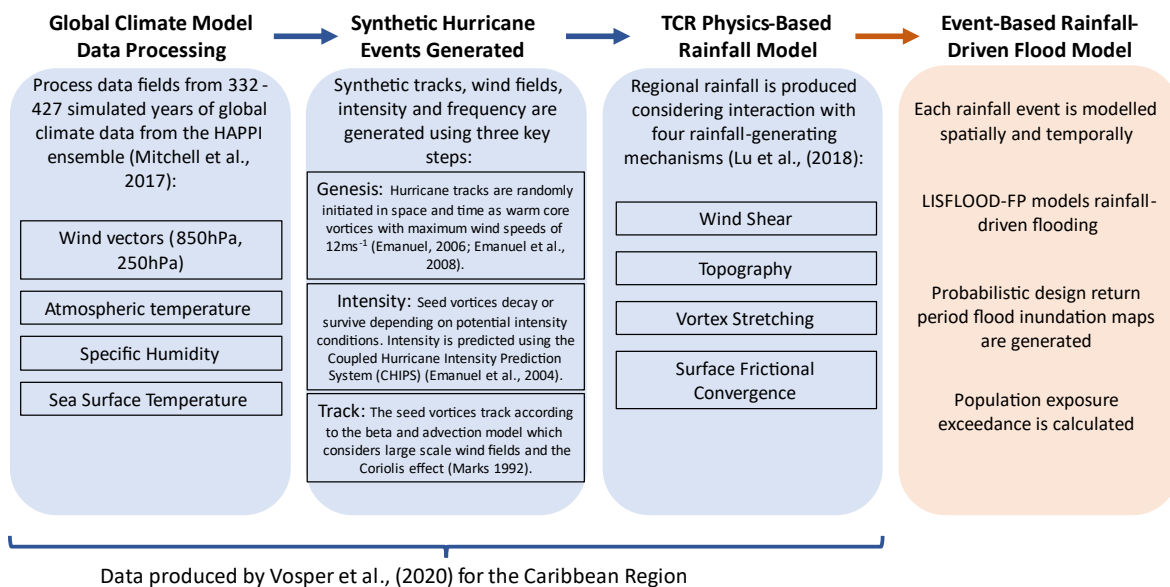
142 To address these questions, we first describe the application of the hurricane rainfall event set in Section 2.1. We
143 explain how the event-based model was set up (Section 2.2), including the novel methodological applications of
144 spatially-varying rainfall in the hydrodynamic model (Section 2.2.1), and the parameterization of river channel
145 bathymetry using the input rainfall event set climatology (Section 2.2.2). In Section 2.3, we describe the
146 combination of population estimates with the flood hazard data to derive population exposure estimates under
147 present day, 1.5°C and 2°C climate change scenarios. The method for validating the model is described in
148 Section 2.4.

149

150 **2.1 Hurricane Rainfall Data**

151 The synthetic hurricane rainfall event set was developed to estimate hurricane rainfall in the Caribbean under
152 present day (2005-2016), 1.5°C and 2°C equilibrated climate change, using a physics-based tropical cyclone
153 rainfall model (Vosper et al., 2020) – see Figure 2. The model produces spatial (10km resolution) and temporal
154 (2-hourly) rainfall estimates along a synthetic hurricane track, considering four key rainfall-generating
155 mechanisms: wind shear, topography, vortex stretching and surface frictional convergence. Inputs to the tropical
156 cyclone rainfall model were atmospheric temperature, specific humidity, sea surface temperature and wind
157 vectors, which are typically taken from Global Climate Models (GCM) or reanalysis products. This model has
158 been validated against gauge-based and radar observations in several studies in the US - including in Puerto
159 Rico - showing good agreement (Feldmann et al., 2019; Lu et al., 2018; Zhu et al., 2013).

160



161

162 **Figure 2 - Diagram outlining the modelling steps involved in simulating the synthetic hurricane rainfall event set and its**
 163 **application in the event-based rainfall driven flood model.**

164

165 To provide driving climate model data to the synthetic hurricane rainfall events under current, 1.5°C and 2°C
 166 climate change, four climate models from the Half A degree additional warming, Prognosis and Projected
 167 Impacts (HAPPI) ensemble were utilised (CanAM4, CAM5-1-2-025degree, NorESM1-HAPPI, ECHAM6-3-
 168 LR: (Mitchell et al., 2017)) - see Table 1. Representative Concentration Pathway (RCP) 2.6 was used for model
 169 boundary conditions at 1.5°C, using a weighted combination of RCP2.6 and RCP4.5 at 2°C. These were
 170 selected based on the availability of variables at the required atmospheric levels with at least daily temporal
 171 resolution for input into the hurricane rainfall model which are described in Figure 2. HAPPI was developed to
 172 document climate change impacts under 1.5°C and 2°C climate change above pre-industrial levels, and has been
 173 a key source of climate data for such studies, including the IPCC Special Report on 1.5°C (IPCC, 2018).

174

175 **Table 1 - Table outlining the resolution of the Global Climate Models used to drive the synthetic hurricane rainfall model**
 176 **from the HAPPI climate ensemble.**

HAPPI Climate Model	Horizontal Resolution	Number of simulated years of climate model data			Reference
		Present day	1.5°C	2°C	
CanAM4	2.81° x 2.81°	332	346	332	Wehner et al., (2014)
CAM5-1-2-025degree	0.31° x 0.23°	409	365	396	Von Salzen et al., (2013)
ECHAM6-3-LR	1.88° x 1.88°	427	378	383	Stevens et al., (2013)
NorESM1-HAPPI	1.25° x 0.94°	423	382	351	Bentsen et al., (2013) Iversen et al., (2013) Kirkevåg et al., (2013)

177 The hurricane rainfall event set consists of 59,000 events, with each climate model scenario equivalent to
178 between 332-427 simulated years of data depending on the climate model (Vosper et al., 2020). 59,000 events
179 were generated corresponding to approximately 5000 events per climate model and climate scenario. For each
180 climate model, the number of simulated years was calculated as the sum of the number of simulated events per
181 year divided by the simulated annual frequency of events in the climate model data (see Table 1). The simulated
182 time period for the present day is 2005-2016, representing a global average temperature of around 0.9°C higher
183 than a pre-industrial climate. The 1.5°C and 2°C time periods are for 2106-2115. This future time period was
184 selected in the HAPPI climate ensemble as the future time slice, chosen to represent a 1.5°C and 2°C world at
185 around 2100 (which was the generally accepted time period for these temperature scenarios in the IPCC Special
186 Report on 1.5°C (IPCC, 2018)), whilst also providing 100 years of simulated GCM data following the present
187 day time slice (2006-2015) (Mitchell et al., 2017). Each synthetic hurricane rainfall event was simulated at a 2-
188 hour time step and 10km spatial resolution before being employed as the input to the event-based rainfall-driven
189 flood model.

190 **2.2 Event-Based Rainfall-Driven Flood Model**

191 LISFLOOD-FP is the hydraulic engine used to simulate channel and floodplain flow in two dimensions in our
192 rainfall-driven hydrodynamic model (Bates et al., 2010; LISFLOOD-FP Developers, 2020). Rainfall is the key
193 input to the model, and water flow is routed in one of two ways. Firstly, very shallow (<1cm) overland flows are
194 routed using a constant-velocity ‘rain on grid’ routing scheme (Sampson et al., 2013). Rain falls directly onto
195 the cells and is routed through the model using a slope-dependent fixed velocity algorithm. Secondly, flow
196 above 1cm deep (i.e. the majority) is routed hydraulically using the inertial form of the shallow water equations
197 (Bates et al., 2010), with river and drainage channels represented using a subgrid approach (Neal et al., 2012).
198 Typical channel (0.035) and floodplain (0.040) manning’s coefficient friction values were applied. As Puerto
199 Rico is an island, all downstream boundaries are the ocean. The downstream boundary conditions in the model
200 are set to sea level, and this could be used in future work to simulate sea level rise and storm surge.

201
202 As Digital Elevation Data is the most important input to a hydrodynamic model (Hawker et al., 2018), LiDAR
203 data was used as the Digital Elevation Model (DEM). LiDAR coverage for Puerto Rico is almost complete
204 (>99%) (United States Geological Survey, 2017) and was resampled from its native 1m resolution to 20m,
205 reprojected to WGS84 and hydrologically conditioned using the Priority-flood method (Zhou et al., 2016). The
206 ~55km² of Puerto Rico not covered by LiDAR was patched with the globally-available MERIT DEM
207 (Yamazaki et al., 2017). This area is mountainous and sparsely populated, meaning the use of MERIT here does
208 not affect the exposure results.

209
210 Whilst high resolution DEMs are important for simulating floods, halving the model grid resolution leads to an
211 increase in simulation time by an order of magnitude (Savage et al., 2016). For example, run on a 2 x 2.6GHz 8-
212 core Intel E5-2670 one example model in this event set for the 9100km² domain covering the entire island of
213 Puerto Rico takes 3 minutes to run at 90m, 77 minutes at 20m, approximately 770 minutes (12.8 hours) at 10m
214 and 7700 minutes (5.3 days) at 1m resolution. As a result, and given we have thousands of events to simulate,
215 the event set was run at 20m. This resolution balances the need for high resolution flood hazard outputs with the
216 computational costs associated with employing a high-resolution event-based model at the island scale, and also

217 reflects state-of-the-art model resolutions used in other locations, such as the UK (Bates et al., 2023). Our study
218 is the first known study to employ an event set approach at such a high hydrodynamic model resolution over
219 such a large domain.

220

221 Infiltration was not included in this model approach for several reasons. As hurricanes take place during the
222 hurricane season (North Atlantic: June – November), soils in Puerto Rico are often saturated meaning
223 infiltration is low (Smith et al., 2005). Many pluvial modelling studies do not include infiltration as the
224 appropriate parameter values are highly uncertain and vary widely across space and time (Bernet et al., 2018;
225 Guerreiro et al., 2017; Hall, 2015). Although antecedent conditions are expected to vary, the infiltration is likely
226 to be of lower importance relative to other factors since infiltration will be minimal under extreme rainfall
227 events - such as those associated with hurricanes (Wehner and Sampson, 2021).

228

229 To improve the representation of islands and hurricane rainfall in the model, two novel model developments
230 were incorporated into the model set up.

231 **2.2.1 Spatially-varying Rainfall**

232 Spatiotemporal representation of rainfall is important for accurate simulation of pluvial flood events (Blanc et
233 al., 2012). Previous pluvial models using LISFLOOD-FP covered only small domains and relied on time-
234 varying but spatially constant rainfall input (Sampson et al., 2013, 2015; Wing et al., 2019). This study
235 demonstrates the first use of spatially and time-varying rainfall in a LISFLOOD-FP rainfall-driven
236 hydrodynamic model, using a new routine to read spatiotemporal rainfall in NetCDF format. For each hurricane,
237 a grid of rainfall at ~10km resolution across the island was input to the model domain at each timestep (2-
238 hourly), although the hydrodynamic model calculations are simulated with much shorter timesteps (order of
239 seconds). To model all 59,000 hurricane rainfall events would be computationally intractable, and was not
240 necessary considering many of the hurricane rainfall events produced no or very little rainfall. Thus, to select
241 events to simulate in the model, all hurricane rainfall events above a threshold of 3.75mmhr^{-1} peak rainfall
242 intensity were simulated - a total of 4909 events (8.3% of total). Within this, 1464 events were present day, 1801
243 events were at 1.5°C and 1644 events were at 2°C . This threshold was selected as the minimum number of
244 events necessary to calculate a robust estimate of the two-year return period flood hazard which is used as the
245 lowest modelled return period event in the event set. Events below this threshold were not considered significant
246 enough in terms of rainfall to run. An additional 8 hours of simulation time was added to the end of each
247 simulation based on our inspection of the time it took for the rainfall to move through the model and reach either
248 the ocean or the lowest points of the DEM. These decisions were based on trial and error and inspection of the
249 rainfall and resulting flood hazard events.

250 **2.2.2 River Channels**

251 Including river channels in flood models is necessary to produce accurate estimates of flood hazard (Hall, 2015;
252 Neal et al., 2021), but most pluvial flood models do not explicitly include river channels or drainage networks
253 (Blanc et al., 2012). Here, a subgrid approach was used to represent river channels and drainage networks in the
254 rainfall-driven modelling framework (Neal et al., 2012). Rivers and drainage channels were represented using
255 the US National Hydrography Dataset v2.1 (Simley and Carswell Jr, 2010). River widths in Puerto Rico are

256 inadequately represented in global hydrographic datasets such as MERIT Hydro (Yamazaki et al., 2019) as most
257 channels are smaller than the resolution of the DEM data used to create such products (e.g. MERIT at 90m in
258 the case of MERIT-Hydro). As a result, width was estimated using a power law regression with upstream
259 accumulated area (Leopold and Maddock, 1953). Widths used here were sampled using satellite imagery along
260 the 13 main rivers across the island. Upstream accumulated area was calculated using the LiDAR DEM at 20m
261 resolution by first generating a flow direction map, and then using the RichDEM algorithm outlined in (Barnes,
262 2017).

263

264 River depth estimates are also unavailable for Puerto Rico, as is typical in most locations globally (Sampson et
265 al., 2015). To parameterise the river channel depths, the present day synthetic hurricane rainfall events for each
266 climate model (total: 1464) were first simulated through a model with arbitrarily deep river channels (-10m) to
267 get estimates of channel water depth for each event. Using these, the water depth at a given return period was
268 calculated empirically. Information on flood defences was also not available, so in this study we parametrize
269 bankfull river depth by calculating the bed elevation to ensure that each channel conveyed the present day one-
270 in-two-year discharge (Pickup and Warner, 1976; Williams, 1978; Wolman and Miller, 1960) generated by the
271 present day hurricane ensemble and subtracted from the bank height derived from the DEM to get a calibrated
272 estimate of the channel depth value. Inevitably this means that in locations where rivers do have defences, the
273 model is likely to overpredict flood hazard. If defence standard information were to become available, it would
274 be a simple matter to retrospectively apply these to the output flood hazard layers.

275

276 **2.3 Population Exposure Estimates**

277 Population exposure was calculated for each flood event as the total number of people exposed to flood depths
278 above 10cm. The WorldPop 90m top-down constrained population dataset (2020) was used to estimate the
279 number of people per 90m grid cell (Tatem, 2017; Bondarenko et al., 2020). WorldPop was chosen because total
280 population estimates are adjusted to 2020 UN population estimates, meaning out-migration trends following
281 Hurricane Maria in 2017 are accounted for. The WorldPop data was downscaled from 90m to 20m to match the
282 flood hazard data, using nearest neighbour resampling and assignment to 20m cells based on a proportional cell
283 method, following (Lloyd et al., 2017). WorldPop has been validated and compared to other datasets extensively
284 (Reed et al., 2018; Leyk et al., 2019; Tuholske et al., 2021), including for flood exposure applications
285 (Mazzoleni et al., 2020; Smith et al., 2019). Smith et al., (2019) found that WorldPop produces larger exposure
286 estimates in comparison to the High Resolution Settlement Layer (HRSL) (Tiecke et al., 2017), likely due to a
287 combination of coarser resolution and assignment of population to buildings. Recently, Tuholske et al., (2021)
288 identified the importance of conducting a sensitivity assessment of gridded population products to capture the
289 inherent uncertainties in the use of gridded population estimates. However, HRSL, High Resolution Population
290 Density Map (HRPDM) (Mapping the world to help aid workers, with weakly, semi-supervised learning, 2020)
291 and WorldPop are likely to give different estimates in our case, not least due to the different dates of the datasets
292 before and after Hurricane Maria, where approximately 8% (230,000) of the population is estimated to have
293 emigrated following the event (Audi et al., 2018). Total population estimates for the main island using HRPDM
294 and HRSL population are 4.87million and 3.66million, which is considerably higher than the UN-adjusted
295 WorldPop estimate of 2.70million, resulting in higher population exposure values. Future population was not

296 considered due to a lack of available high-resolution datasets (<100m grid size) estimating changes in future
297 population. For consistency, population exposure exceedance was calculated for each event using the same
298 method as the hurricane rainfall as 1/Annual Exceedance Probability (Emanuel and Jagger, 2010; Feldmann et
299 al., 2019; Vosper et al., 2020).

300

301 **2.4 Model Validation**

302 To determine the skill of our flood hazard estimation, we assessed model performance using high water mark
303 (HWM) data collected by USGS following Hurricane Maria (available here:
304 <https://stn.wim.usgs.gov/FEV/#MariaSeptember2017>). For more information about the suitability assessment of
305 the HWM data for validation, see Text S1 and Table S2. See Figure S1 for the HWM locations used in this
306 study. Ideally it would be better to validate the event set with a lower magnitude flood considering the focus of
307 this work is primarily on on low-magnitude, high-frequency events. However, there is no known validation data
308 for small hurricane rainfall-driven flood events in Puerto Rico. As a result, Hurricane Maria was chosen as the
309 event to validate against despite its high magnitude.

310

311 Firstly, to produce flood hazard estimates of Hurricane Maria for validating the model and event set, we ran the
312 hydrodynamic model using two observational rainfall products (IMERG and NCEP Stage IV) that provide
313 space-time varying estimates of Hurricane Maria rainfall through the flood inundation model. We use an
314 identical hydrodynamic model set-up to the event set, only changing the input rainfall data. IMERG (IMERG:
315 Integrated Multi-satellitE Retrievals for GPM | NASA Global Precipitation Measurement Mission, 2023) was
316 run at ~10km spatial resolution, and at 30-min intervals, whilst NCEP Stage IV (NCEP/EMC 4KM Gridded
317 Data (GRIB) Stage IV Data, 2023) was run at ~4km spatial resolution, with an hourly temporal resolution.
318 NCEP Stage IV was used instead of the higher resolution Multi-Radar Multi-Sensor (MRMS) rainfall product as
319 the landfall year of Hurricane Maria (2017) falls outside of the MRMS archive period (2020-onwards) (MRMS
320 Operational Product Viewer, 2023).

321 We compare the flood hazard produced using IMERG and NCEP Stage IV to understand the uncertainty in
322 flood hazard estimates using the different observation inputs.

323

324 IMERG has been widely compared to gauge-based rainfall data over many locations globally, demonstrating
325 good performance in estimation of total rainfall (Freitas et al., 2020; Pradhan et al., 2022), as well as good
326 representation of temporal (Yu et al., 2021) and spatial event structure (Omranian et al., 2018; Rios Gaona et al.,
327 2018; Pradhan et al., 2022). For example, Rios Gaona et al., (2017) shows IMERG has a low relative bias over
328 the Netherlands (-1.51%), and Tan et al., (2017) reports a correlation coefficient of 0.78 against radar and
329 gauge-based observations in the United States. IMERG has also been shown to perform well at capturing
330 rainfall from tropical cyclones (Rios Gaona et al., 2018; Yu et al., 2021). For example, Omranian et al., (2018)
331 found IMERG correctly predicted 62% of rainfall from Hurricane Harvey. Nonetheless, some studies have
332 identified a tendency for IMERG data to underpredict rainfall intensity during extreme rainfall events (Freitas et
333 al., 2020; Mazza and Chen, 2023; Tian et al., 2018; Yu et al., 2021). For example, Yu et al., (2021) found that
334 extreme precipitation rates from IMERG were 7.53% lower than gauge data for Typhoon Lekima in 2019.

335

336 NCEP Stage IV is a ground-based gauge and radar observation product that is often used in multi-product
337 comparison studies as the baseline observed dataset (Nelson et al., 2016). These studies have demonstrated that
338 NCEP Stage IV produces good representation of overall rainfall rates across the United States (Nelson et al.,
339 2016; Prat and Nelson, 2015), as well as the spatial and temporal structure of rainfall (Habib et al., 2009);
340 including for tropical cyclones (Gao et al., 2020; Villarini et al., 2011). Prat and Nelson, (2015) compare annual
341 rain rate for the conterminous United States using NCEP Stage IV against gauge data, finding a correlation
342 coefficient of 0.93 (R^2). Gao et al., (2020) show that NCEP Stage IV only overestimated rainfall from Hurricane
343 Harvey by 2%. However, underestimation of extreme rainfall has been shown in some studies due to an increase
344 in the number of missed events as rain rate increases (Habib et al., 2009; Prat and Nelson, 2015). For example,
345 Prat and Nelson, (2015) report that NCEP Stage IV has a tendency to underestimate rainfall in comparison to
346 surface observations across the conterminous United States (-14%- +1% depending on location). This is likely a
347 product of the inherent limitations of radar-based precipitation products (see Nelson et al., (2016)).

348

349 The model used to produce the synthetic hurricane rainfall event set utilized in this study has previously been
350 compared to NCEP Stage IV data over Puerto Rico, showing very good agreement (Feldmann et al., 2019). This
351 demonstrates the suitability of the use of NCEP Stage IV as an observation dataset for comparison against in
352 this study. Omranian et al., (2018) showed IMERG was able to represent 62% of rainfall from Hurricane Harvey
353 in comparison to NCEP Stage IV, thus suggesting that IMERG is also likely capable of adequately representing
354 extreme rainfall associated with Hurricane Maria. However, the performance of IMERG and NCEP Stage IV
355 data can be dependent on the number of gauge-based observations available (Tang et al., 2018; Tian et al.,
356 2018). 14 out of 24 USGS gauges were damaged during Hurricane Maria in Puerto Rico (Bessette-Kirton et al.,
357 2020). As a result, this is a key limitation of using observed data products to estimate tropical cyclone rainfall
358 that should be considered when drawing conclusions about the accuracy of flood hazard associated with these
359 rainfall products.

360

361 Next, we compared the performance of the event set against the HWM data and the estimates from the observed
362 rainfall products to sense check the model. Hurricane Maria-like events were identified across all model
363 scenarios first by maximum total rainfall, and then by spatial characteristics of the hurricane track. Maximum
364 total rainfall is defined as the highest total rainfall accumulation at a point on the island. This metric was used as
365 opposed to mean total rainfall, as studies that have investigated Hurricane Maria rainfall describe the maximum
366 total rainfall as the most significant anomaly in the historical record associated with the event (Ramos-Scharrón
367 and Arima, 2019; Keellings and Hernández Ayala, 2019; Pokhrel et al., 2021). Maximum total rainfall is also
368 the metric used to estimate the return period of Hurricane Maria rainfall; at least a 1-in-115-year rainfall event
369 (Keellings and Hernández Ayala, 2019). Studies use different metrics to derive maximum total rainfall,
370 including interpolation of rain gauge data and observation products such as NCEP Stage IV. This means that the
371 maximum total rainfall for Hurricane Maria varies between studies, ranging between 733-1029mm (Pasch et al.,
372 2018; Keellings and Hernández Ayala, 2019; Ramos-Scharrón and Arima, 2019; Pokhrel et al., 2021). There are
373 a limited number of events in our event set with a >100-year return period magnitude maximum total rainfall
374 (mean: 3.46 samples per climate model scenario) due to the comparatively short simulated time record of our
375 event set (range: 332-427 years). However, Puerto Rico experiences on average one hurricane each year, and

376 has a mean annual rainfall of over 4000mm in some locations (Hernández Ayala and Matyas, 2016). There are
377 therefore many events in the event set with total mean rainfall (total accumulated rainfall averaged across the
378 island) in the range of Hurricane Maria (range: 375-380mm (Pokhrel et al., 2021; Keellings and Hernández
379 Ayala, 2019; Ramos-Scharrón and Arima, 2019)). However, these events have widely varying spatial
380 characteristics and associated flood hazard and are therefore not all are Maria-like. Thus, it is also important to
381 consider the spatial characteristics of the hurricane rainfall events so that events with similar rainfall and spatial
382 characteristics to Hurricane Maria can be identified. Similarity to Hurricane Maria based on track location was
383 assessed based on four criteria: i) direct landfall on the main island; ii) south-western trajectory; iii) makes
384 landfall on the eastern portion of the main island; and iv) similar track trajectory across the island, whereby the
385 event track and Hurricane Maria track intersect at at least one point on the island.

386 **3 Results**

387 **3.1 Hurricane María Model Validation**

388 Figure 3 shows the flood hazard estimates produced by simulating the IMERG and NCEP Stage IV rainfall
389 products spatiotemporally through the flood inundation model from the island to local scale. The RMSE
390 between the modelled flood hazard and the HWM is 1.18m for IMERG and 1.22m for NCEP Stage IV (see
391 Figure 4). This is comparable to post-event HWM validation done in other locations (Wing et al., 2021) (see
392 Section 4.1 for discussion of this). There is a significant difference in the flood extents produced using IMERG

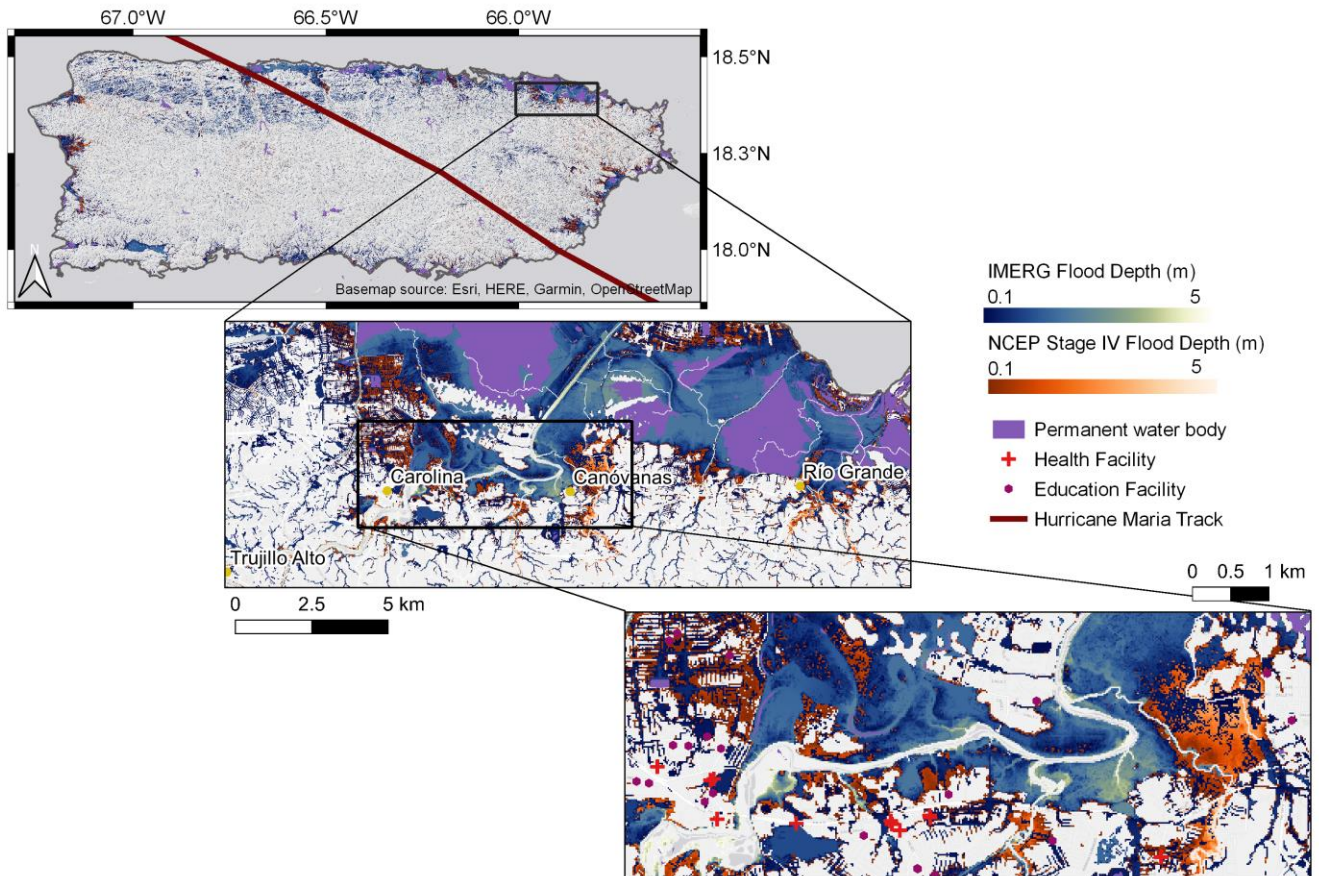


Figure 3 - Map showing the differences between flood hazard estimates of Hurricane Maria produced using IMERG and NCEP Stage IV precipitation data from the island to local scale.

393 and NCEP Stage IV, with larger areas flooded using NCEP Stage IV than IMERG. This highlights the
 394 uncertainty in so-called ‘observed’ flooding from Hurricane Maria.

395 In the event set, when the spatial characteristics of the hurricane rainfall events are considered in addition to the
 396 maximum total rainfall, events we select as Hurricane Maria-like events have some of the lowest RMSEs
 397 between the observed and modelled water surface elevations (range: 1.13-1.33m) as demonstrated in Figure 4.
 398 The track locations of these events are shown in Figure S2. The relationship between maximum total rainfall
 399 and RMSE for all events is expected, whereby as the intensity of the event increases, the sensitivity to the flood
 400 depths decreases as the floodplain fills and thus becomes less responsive to additional increases in rainfall
 401 (Wing et al., 2021). However, there are events in the event set with both much higher and lower rainfalls than
 402 Hurricane Maria that have both similar and very different RMSEs to the Maria-like events. This demonstrates
 403 the importance of the spatial characteristics of the events beyond just the rainfall.

404

405 When comparing the flood estimates using IMERG and NCEP Stage IV against the High Water Mark data, the
 406 event set Maria-like events have similar RMSE scores (Figure 4). However, both observational rainfall products
 407 have different maximum total rainfalls than those found in the literature. In particular, the IMERG maximum
 408 total rainfall is considerably lower. This is likely because satellite products such as IMERG often underestimate
 409 orographic rainfall such as that exhibited over Puerto Rico (Dinku et al., 2008).

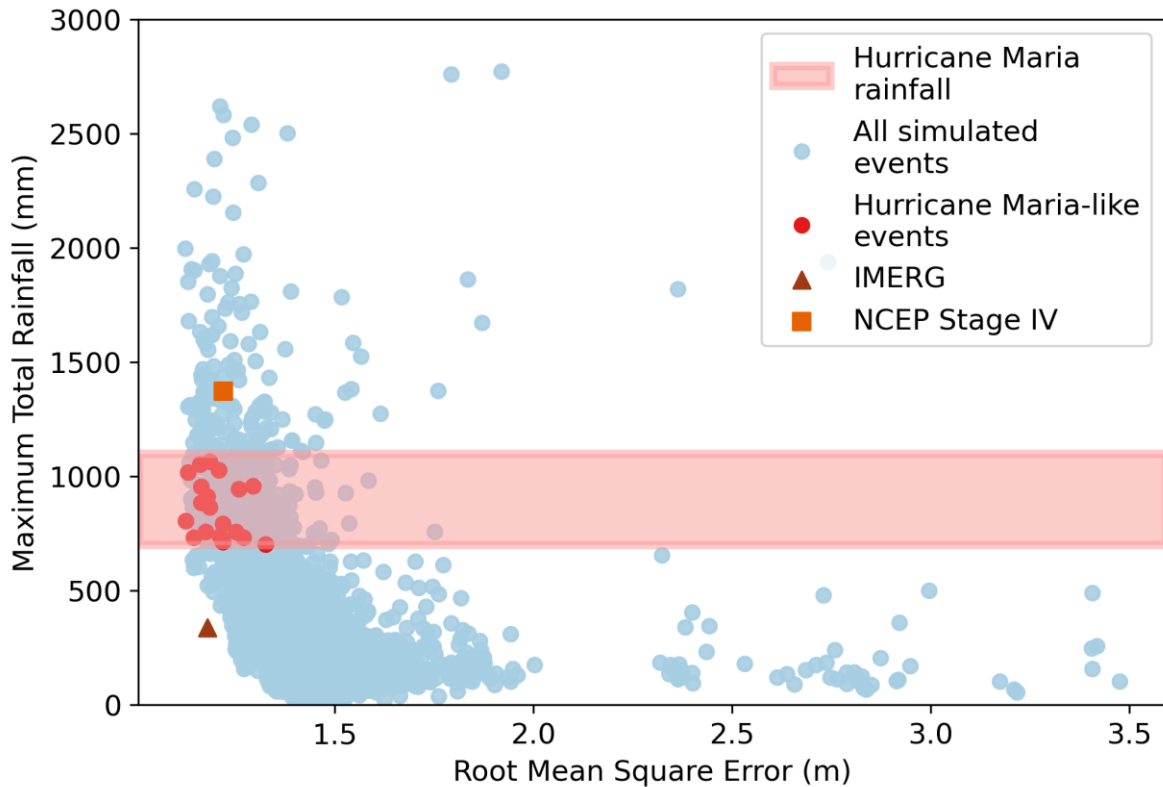


Figure 4 - Graph showing the relationship between Root Mean Square Error (RMSE) and maximum total rainfall for all simulated events under all climate scenarios (4909 events total). Blue = all simulated events. Red = events identified with Hurricane Maria maximum rainfall totals and spatial characteristics (20 events). Red band = range of reported Hurricane Maria rainfall. Orange square = NCEP Stage IV model. Brown triangle = IMERG model.

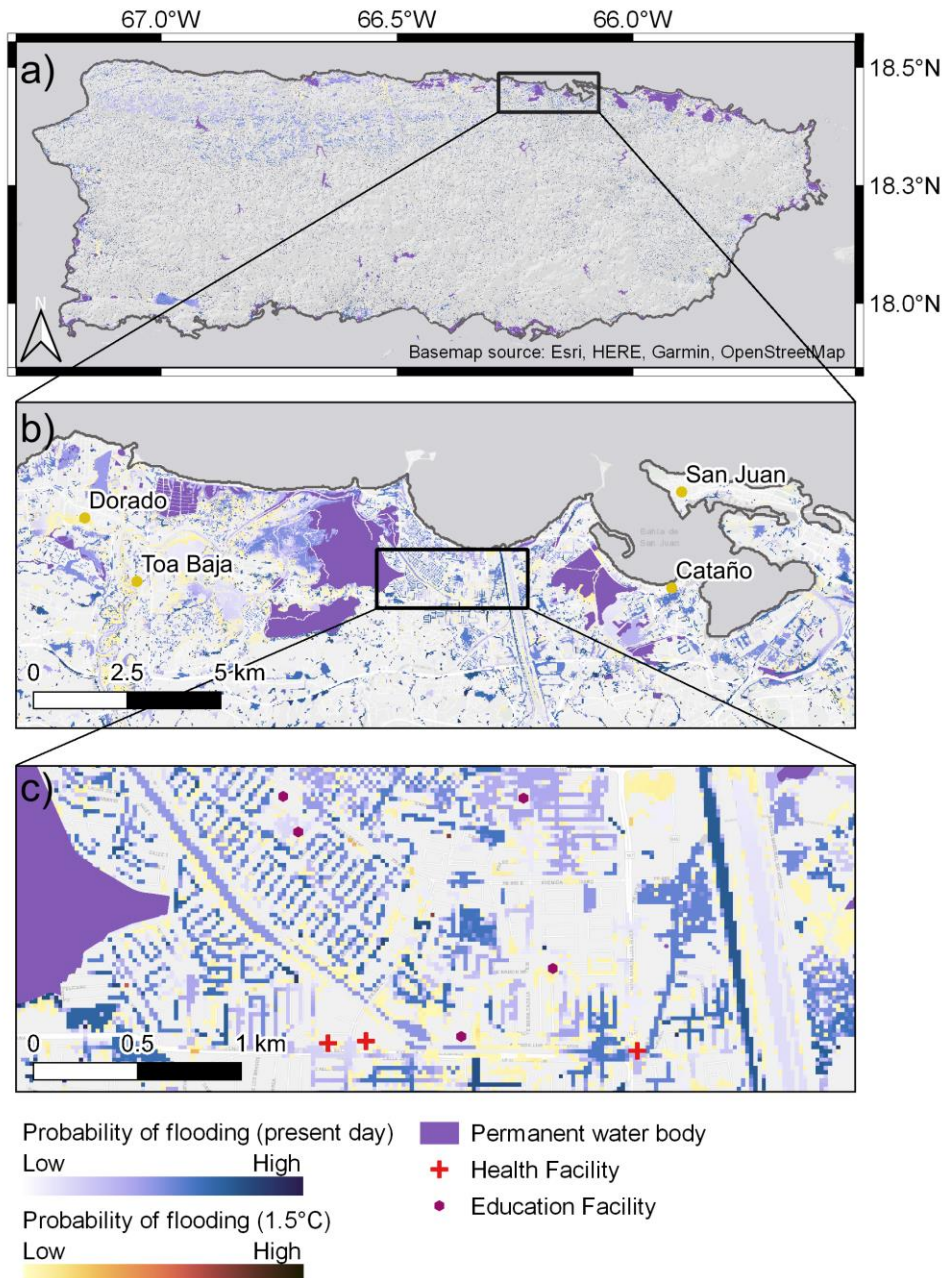
411 3.2 Design Return Period Flood Hazard Maps

412 The probability of inundation was calculated for each pixel in the model domain, calculating how many times
 413 each pixel would be inundated above a 10cm depth in each climate model temperature scenario. The return
 414 period of inundation in each pixel was then determined, by calculating how many times we expect a pixel to
 415 flood based on the number of years of data simulated (range: 332-427 years depending on the climate model).
 416 Using this, we derived a set of return period flood hazard maps, which provide a spatially explicit representation
 417 of a given return period flood event under present day, 1.5°C and 2°C warming. This supersedes any currently
 418 available hurricane rainfall-driven flood risk information in Puerto Rico, both under current and future climate
 419 change. This approach also moves beyond the traditional uplift approach often used in flood risk assessment
 420 under climate change, as it provides spatially explicit flood hazard information for a given return period at the
 421 island scale and at high resolution.

422

423 Figure 5 highlights the scale and detail of flood hazard information using this approach, from the island scale
 424 (Figure 5a) to the local scale (Figure 5c). For example, Figure 5c shows flooding at the street level in Levittown,
 425 Toa Baja – a town significantly impacted by flooding from Hurricane Maria in 2017 (Major Hurricane Maria -
 426 September 20, 2017).

427



428

429

430

431

432

Figure 5 - Map showing the 20-year return period flood based on probability of inundation under present day and 1.5°C climate change for the ECHAM6-3-LR climate model. a) Flooding at the island scale. b) Flooding in the Toa Baja and Cataño districts. c) Flooding in Levittown, Toa Baja. For presentation purposes, only inundation probabilities at present day and 1.5°C are shown here.

433

434

435

436

437

438

439

440

Based on this example for a 20-year return period flood hazard event using the ECHAM6-3-LR climate model, several schools and hospitals would likely be impacted under present day and 1.5°C climate change. The estimated flooded area of the 20-year return period flood increases under 1.5°C climate change in comparison to present day (2006-2015) (Figure 5c), meaning areas currently not at risk are affected at 1.5°C climate change. Changes at 2°C are similar to 1.5°C, but are not shown in Figure 5 for presentation purposes.

Flooding in the northwest of the island shown in Figure 5a (latitude/longitude location: 18.3,-67.0 to 18.4,-66.5) is a feature of the topography and model structure, not data error. This area is dominated by karst hydrology

441 (Hughes and Schulz, 2020). Therefore, these areas of pooled water would likely not feature if karst processes
442 were explicitly represented in the model set up. The inclusion of karst processes was beyond the scope of this
443 study, and as this area is sparsely populated it is unlikely to impact the estimates of population exposure
444 presented.
445

446 **3.3 Characterising Changes in Population Exposure Under Present Day, 1.5°C and 2°C**

447 This research estimates changes in population exposure to hurricane rainfall-driven flooding for the island of
448 Puerto Rico under present day, 1.5°C and 2°C climate change. The climate change scenarios are analysed for
449 each individual climate model, as opposed to the aggregate results, as there are important differences between
450 models that are obscured when using the mean. This is a way of investigating uncertainty explicitly, by
451 understanding the differences between models. Studies such as Daron et al., (2021) have highlighted the
452 importance of assessing individual model performance when climate models give a wide range of projections.
453

454 Figure 6 shows the return period of a given exceedance of population exposure from hurricane rainfall-driven
455 flooding in Puerto Rico under present day, 1.5°C and 2°C climate change. Return periods of population
456 exposure exceedance above the 30-year return period are not considered and are thus faded in Figure 6. The
457 number of samples for each climate model scenario above the 30-year return period is too small (mean: 12.7
458 samples) to determine accurate estimates of population exposure above the 30-year return period (see Figure 6).
459 Thus, changes in population exposure above the 30-year return period in this event set are subject to significant
460 uncertainty resulting from limited samples at these event magnitudes and are therefore not considered further in
461 this analysis. A much longer event set would be required to simulate robust changes in population exposure at
462 higher magnitude return periods.
463

464 Three of the four climate models show agreement in the direction of change between present and future climate
465 change, with increases in population exposure associated with a given return period at 1.5°C and 2°C compared
466 to present day. However, one climate model (CanAM4) shows the opposite trend above the 10-year return
467 period (see Figure 7). One key reason for this is likely to be the differences in resolution of the underlying
468 Global Climate Model (GCM) data: CanAM4 GCM has a coarser resolution ($2.81^{\circ} \times 2.81^{\circ}$) than the next most
469 coarse GCM ECHAM6-3-LR ($1.88^{\circ} \times 1.88^{\circ}$) (see **Table I**). As a result, the underlying variables driving extreme
470 hurricane rainfall are less likely to be well-represented in CanAM4 compared to the other three climate models.
471 It is well understood that higher-resolution GCMs are better able to simulate the underlying conditions
472 important for the development of extreme rainfall and tropical cyclones (Knutson et al., 2020).

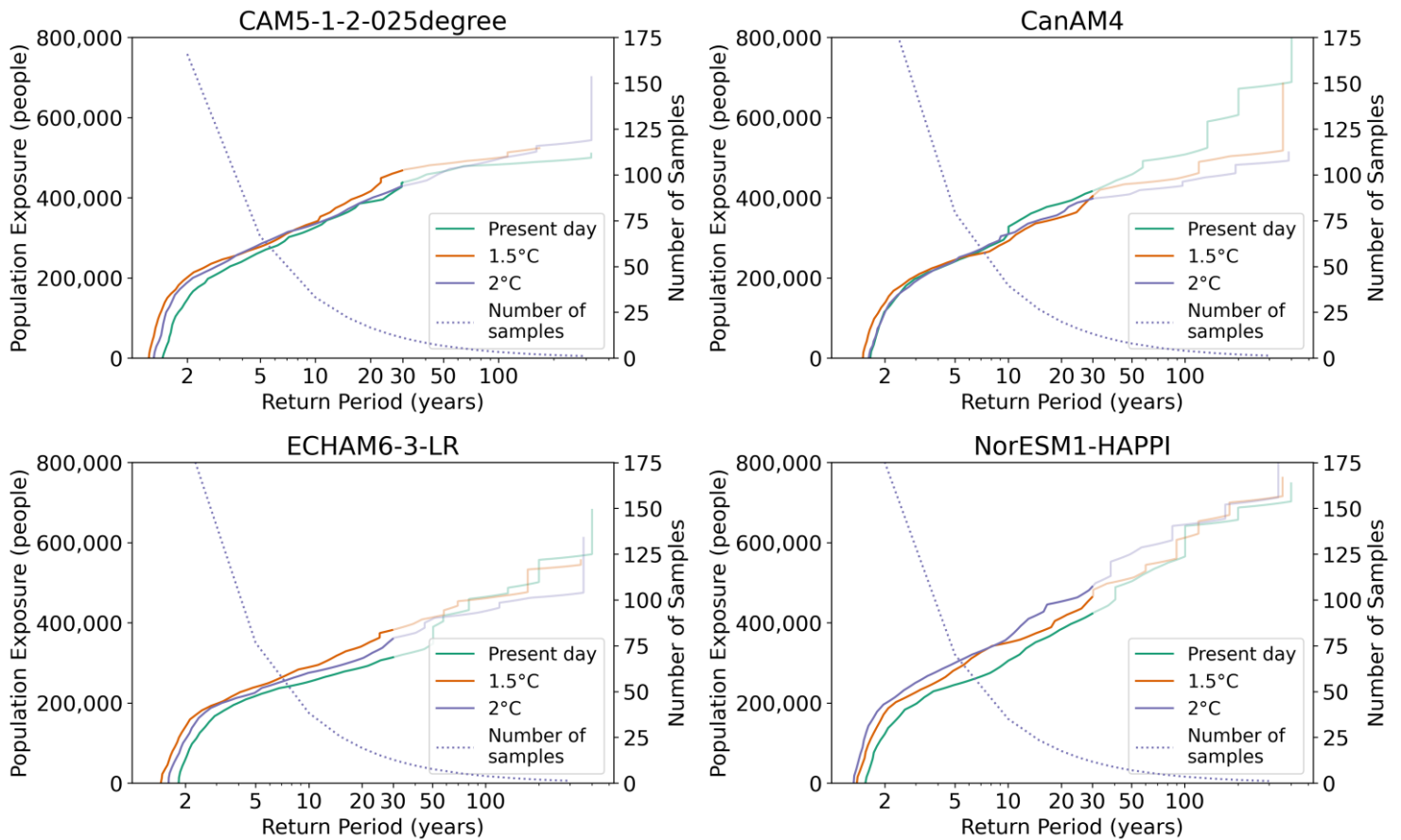


Figure 6 - Graph showing population exposure exceedance for present day, 1.5°C and 2°C climate change, as well as the number of samples in each climate model at a given return period (dotted line). Population exposure above the 30-year return period is faded to represent the uncertainty associated with the limited number of samples at these return periods.

473

474 Present day population exposure to flooding from hurricane rainfall in Puerto Rico is approximately 2-5% at the
 475 two-year return period, rising to 8-10% at the five-year, 9-12% at the ten-year and 11-14% at the twenty-year
 476 return periods respectively (see Figure 6). These are the first published estimates of present day population
 477 exposure from flooding in Puerto Rico. It is difficult to corroborate population exposure estimates with those for
 478 previous events in Puerto Rico due to a lack of data, however these estimates are plausible given the universal
 479 island-wide flash flood warning given to Puerto Rico during Hurricane Maria (Pasch et al., 2018).

480

481 As shown in Figure 7, the estimated number of people exposed to flooding from hurricane rainfall on average
 482 every two years would increase by the largest percentage across the different return periods (20-140% at 1.5°C;
 483 -3-85% at 2°). The lower bound here represents the results from the CanAM4 model, which has the lowest
 484 GCM resolution (see Table 1). The reason for the widest range at the two-year return period could be because of
 485 the different bed elevations sized at the historical two-year return period for each climate model. For a return
 486 period population exposure of five years as shown in Figure 8, the percentage increase in population exposure at
 487 1.5°C and 2°C ranges from 2-15% and 1-20%, respectively. This is a considerably lower range than the
 488 population exposure exceedance at the two-year return period, but also shows more agreement between the
 489 climate models.

490 As shown in Figure 7 there is a notable difference in population exposure exceedance between present day and
 491 1.5°C in three of the four climate models, but a less clear difference between 1.5°C and 2°C. In two of the four
 492 climate models (CAM5-1-2-025degree and ECHAM6-3-LR), the percentage of population exposed at a given
 493 return period is higher at 1.5°C compared to 2°C, and in one climate model (NorESM1-HAPPI), higher at 2°C
 494 compared to 1.5°C. In the CanAM4 climate model, depending on the return period, the percentage of population
 495 exposure varies between the three climate scenarios, and no consistent pattern is shown between the three across
 496 different return periods.
 497

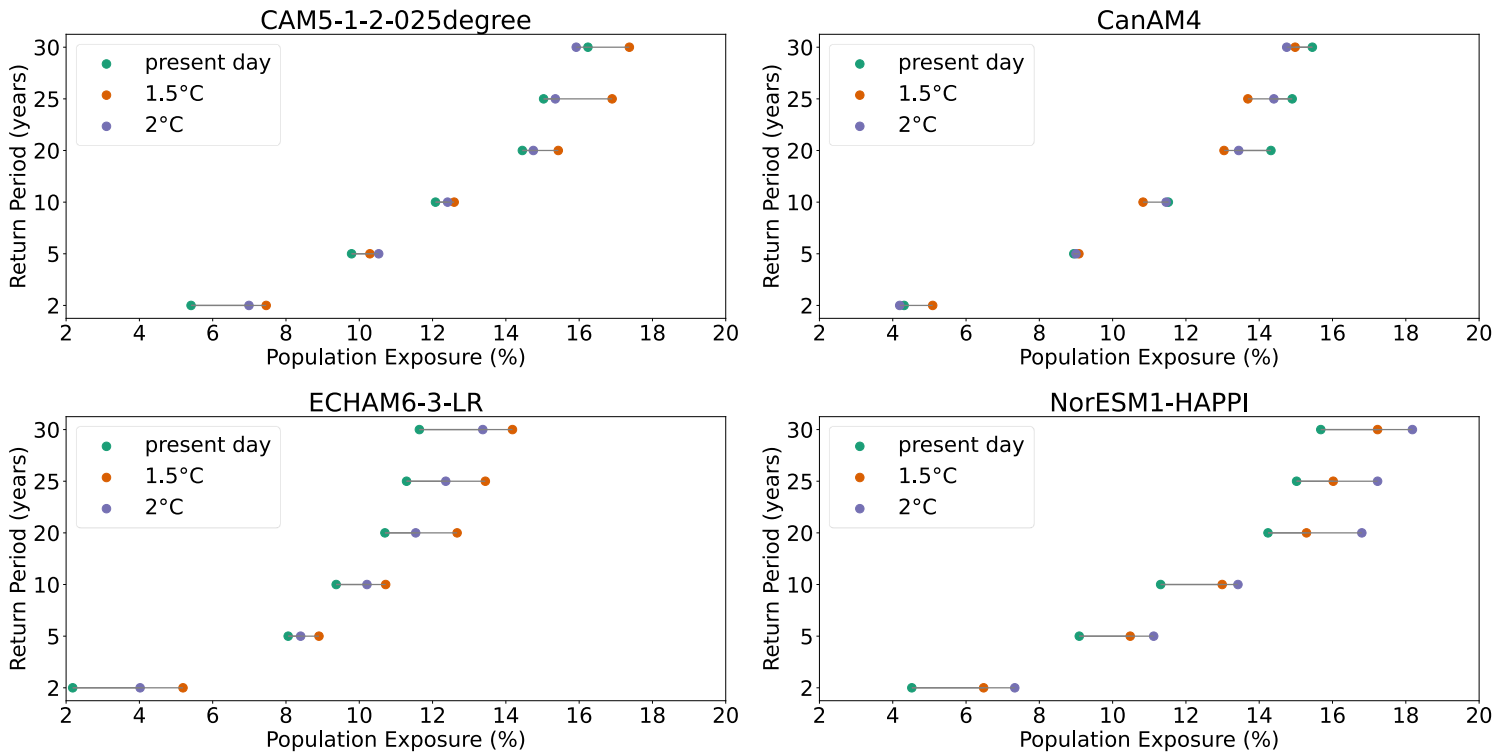
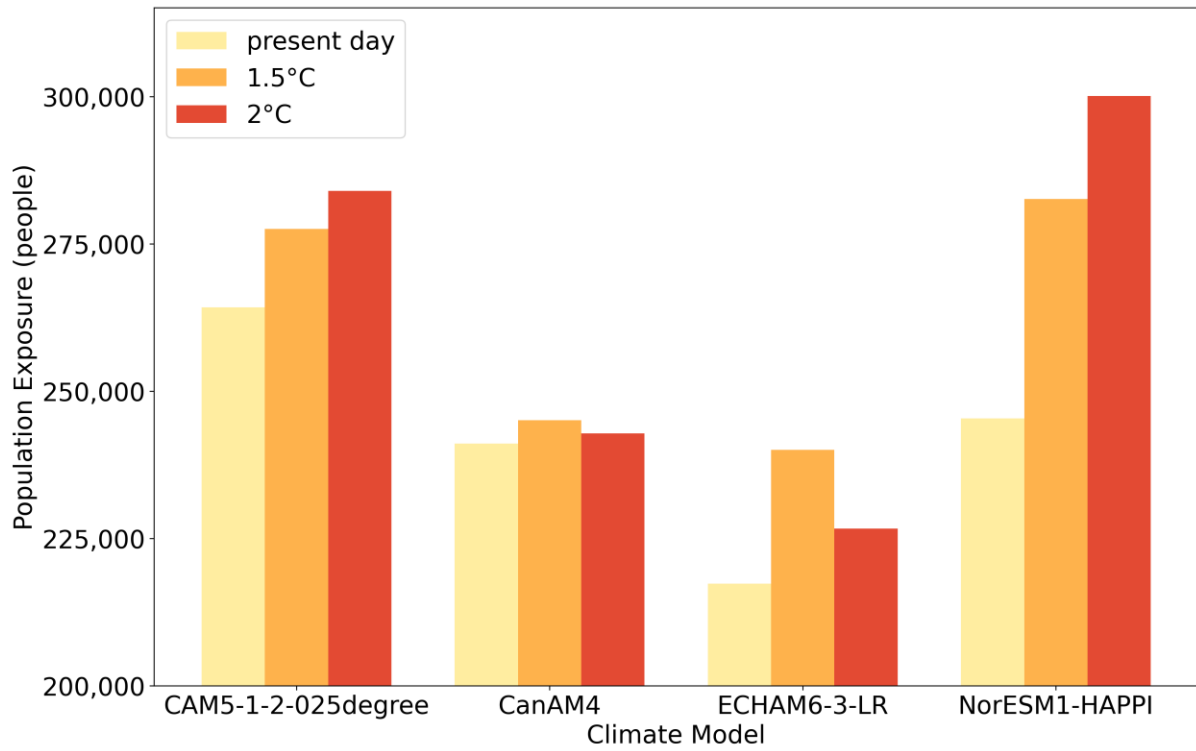


Figure 7 - Plot showing the percentage of population exposed to flooding under present day, 1.5°C and 2°C climate change, and the difference between the three scenarios for each HAPPI climate model. The green dot represents present day population exposure (as a percentage of the total population), with the orange and purple dots representing the population exposure (%) at 1.5°C and 2°C. The difference between the population exposure between the different scenarios is represented by the line between the dots.

498
 499 Figure 8 demonstrates that the range in absolute population exposure numbers estimated for a given return
 500 period between the four climate models is the same as or greater than the percentage uplift in population
 501 exposure associated with 1.5°C and 2°C, highlighting the range of possible absolute population exposure
 502 estimates. For the 5-year return period, present day absolute population exposure ranges from 217,000
 503 (ECHAM6-3-LR) to 264,000 (CAM5-1-2-025degree). This is a 21% difference, whereas the highest population
 504 exposure increase is 22% between present day and 2°C for the NorESM1-HAPPI climate model. This
 505 underlines the difficulty in estimating current population exposure to flooding. This is not only the case in data-
 506 sparse areas such as Puerto Rico, but also in data-rich areas such as the conterminous US (Bates et al., 2021).
 507 However, the direction of change between the ‘present day’ and ‘future’ climate change (1.5°C and 2°C) is
 508 robust across three of the four climate models, meaning the signal in population exposure to flooding is
 509 observable when comparing present day and future climate change, despite the uncertainty in absolute terms.



511

512 **Figure 8 - Bar graph showing the number of people exposed to flooding under present day, 1.5°C and 2°C climate**

513 **change for the 5-year population exposure exceedance for each HAPPI climate model.**

514 **4 Discussion**

515 Our estimates of flood hazard and population exposure driven by hurricane rainfall under current and future climate
516 change supersedes previous efforts to estimate hurricane rainfall-driven flood risk in Puerto Rico. Previous estimates
517 rely on local-scale FEMA fluvial assessments or the global large-scale assessments that most often neglect small
518 islands through choice of scale. Although, the FEMA models will likely be more accurate locally where they exist,
519 depending on the local river channel and flood defence information that was available to the model developers. This
520 research is one of the first known published studies which propagates spatially and temporally explicit hurricane
521 rainfall through to the impact modelling of flood hazard and population exposure estimates, and the first in a small
522 island. Utilising hydrodynamic flood models to understand changes in flooding under climate change is a critical
523 gap in the literature, despite the widespread use of hydrodynamic models to assess current flood risk. The latest
524 IPCC AR6 Working Group I report demonstrated that changes in rainfall were still the dominant method used to
525 assess changes in pluvial flooding under climate change (Seneviratne et al., 2021). However, here we find that the
526 changes in population exposure between present day and 1.5°C and 2°C climate change do not correspond linearly
527 with changes in hurricane rainfall using the HAPPI climate models (Vosper et al., 2020) analysed here, and
528 therefore this rainfall proxy method may not be appropriate when investigating changes in flooding from hurricane
529 rainfall.

530 **4.1 Validating an Event-Based Model**

531 We present the first estimates of rainfall-driven flooding from Hurricane Maria using IMERG and NCEP Stage IV
532 precipitation data. Comparison against HWM data from Hurricane Maria showed that the RMSE of these estimates
533 was reasonable given the typical uncertainties in data of this type (IMERG: 1.18m, NCEP Stage IV: 1.22m). There
534 is uncertainty associated with the HWM vertical datum transformation using VDatum (+/-0.92m) which is likely to
535 impact the RMSE. However, these RMSEs have a similar magnitude to studies conducted in data-rich regions with
536 similar quality HWM data, such as the conterminous US (~1m) (Wing et al., 2021). This demonstrates that the
537 model is capable of realistically simulating flood depths, and thus the suitability of the model for estimating flood
538 hazard under current and future climate change. Inevitably, this finding should be considered alongside the inherent
539 limitations when comparing flood estimates to High Water Mark data. For example, RMSEs in this study are higher
540 than in studies such as Neal et al., (2009) (RMSE: 0.28m). Yet, the HWM data in this study is arguably lower
541 quality data due to the catastrophic nature of the hurricane which limited accessibility for post-event assessment due
542 to wide scale infrastructure failure (Main et al., 2021). HWMs in this study are concentrated in populated areas, and
543 were probably constrained to where it was safe to travel immediately post-event. The performance of the model is
544 likely biased towards these coastal, more populated areas. However, this is also where a considerable portion of the
545 risk is on the island, as this is where the majority of the population resides.

546

547 Moreover, there are limitations of the observation precipitation datasets used, which propagate into the flood
548 estimates. Many studies have compared the performance of NCEP Stage IV and IMERG rainfall data (Li et al.,
549 2022; Mazza and Chen, 2023; Omranian et al., 2018; Villarini et al., 2011). Tropical cyclone precipitation in the

550 conterminous United States between 2002-2019 was much higher in NCEP Stage IV than in satellite products such
551 as IMERG (Mazza and Chen, 2023). Other studies support this conclusion and find that the explanation for this
552 difference is more likely an underestimation of other products, and not an overestimation bias in NCEP Stage IV
553 itself (Villarini et al., 2011). For example, IMERG is likely to underestimate orographic rainfall, which could
554 explain why the flood extent using IMERG is lower than using NCEP Stage IV (see Figure 3). This provides an
555 incentive for the event set approach outlined in this study, as it allows a consideration of a wider range of plausible
556 events to get a greater understanding of uncertainty than just the observed.

557
558 Based on the events selected as Hurricane Maria-like highlighted in Figure 4, we find that our event set contains
559 those like Hurricane Maria, and that these events have amongst the lowest RMSE in comparison to observed HWMs
560 from Hurricane Maria (range: 1.13-1.33m). It was expected that given the extreme magnitude of Hurricane Maria
561 (~115 year return period hurricane rainfall event: (Keellings and Hernández Ayala, 2019)), there would be a limited
562 number of events in our event set with this magnitude due to the comparatively short, simulated time record of our
563 event set (range: 332-427 years per climate model scenario). In our event set across all climate model scenarios, we
564 find 20 events that we classify as Hurricane Maria-like based on maximum total rainfall and spatial characteristics.
565 This finding firstly reinforces just how extreme Hurricane Maria was, following both the devastating impact on the
566 population and infrastructure (Audi et al., 2018; Michaud and Kates, 2017; Main et al., 2021), as well as the
567 literature examining the event in the context of the historical record (Keellings and Hernández Ayala, 2019; Ramos-
568 Scharrón and Arima, 2019). This also indicates that the model has the capacity to replicate events such as Hurricane
569 Maria when both maximum total rainfall and spatial characteristics are considered. Two key conclusions can be
570 taken from this. Firstly, this highlights the importance of variables other than rainfall when estimating rainfall-
571 driven flooding, such as spatial characteristics of the hurricane including landfall location and trajectory. Just
572 considering the rainfall was not sufficient to identify Maria-like events. As a result, simulating the spatial and
573 temporal distribution of the rainfall in an event set is a crucial step needed to accurately represent the relationship
574 between hurricane rainfall and flood hazard in Puerto Rico. This finding reinforces previous research which
575 identifies the importance of hurricane landfall and spatial location on the generation of floods in Puerto Rico
576 (Hernández Ayala et al., 2017; Hernández Ayala & Matyas, 2016; Smith et al., 2005). Secondly, considering there is
577 uncertainty in so-called observed flooding from Hurricane Maria (see Figure 3), the event set provides the
578 opportunity to assess many more realisations of events with similar characteristics to Hurricane Maria than available
579 just using observations. This may allow a better understanding of uncertainty in rainfall-driven flooding for a given
580 event, and thus a greater understanding of risk. Future research investigating changes in flooding from hurricane
581 rainfall should thus take an event-based approach as outlined in this study.

582 **4.2 Current Population Exposure to Flooding from Hurricane Rainfall**

583 Our results highlight the first published estimates of population exposure to flooding in Puerto Rico under the
584 present day climate, with approximately 8-10% of the population currently exposed to flooding from hurricane
585 rainfall at the five year recurrence interval. This level of population exposure has important implications for
586 resilience to floods. It also underlines the exposure to hydrometeorological hazards already experienced in SIDS,

587 which is a key reason for their high risk to climate change and disasters (Thomas et al., 2020). It is also worth noting
588 that these population exposure estimates are for the present day (2005-2016) climate at around 0.9°C of global mean
589 warming and therefore do not represent a pre-industrial climate. This means population exposure estimates for the
590 present day identified in this study are likely to be already influenced by climate change, given the significant
591 impact of climate change found on recent hurricane rainfall events in Puerto Rico such as Hurricane Maria
592 (Keellings and Hernández Ayala, 2019; Patricola and Wehner, 2018).

593 **4.3 Population Exposure to Flooding from Hurricane Rainfall Under 1.5°C and 2°C Climate Change**

594 The results presented in this research estimate that population exposure to flooding from hurricane rainfall will be
595 amplified under 1.5°C and 2°C in all but one of the four HAPPI climate models analysed. The Paris Agreement
596 includes the 1.5°C target as the higher ambition goal and is often touted as our best chance to limit the impacts of
597 climate change to within a 'safe limit'. However, our analysis contributes to the discourse SIDS have been
598 highlighting for some time now, which is that even a 1.5°C temperature rise above preindustrial levels leads to a
599 serious threat to the adaptive capacity (Ourbak and Magnan, 2018; Mycoo, 2018; Hoegh-Guldberg et al., 2018;
600 Mycoo et al., 2022). Here, we find that even at 1.5°C, the increase in population exposure associated with hurricane
601 rainfall-driven flooding in Puerto Rico is enhanced for events with a return period below 30 years. This may have
602 wide-reaching implications for the resilience of Puerto Rico's population. Moreover, although the 1.5°C goal is
603 technically feasible (IPCC, 2018, 2021), it is not currently the most likely temperature rise based on existing policy
604 pledges. At the time of writing, global temperature increase has already reached ~1.1°C above pre-industrial levels
605 (World Meteorological Organization, 2021). Based on our analysis, it is likely that flood hazard and population
606 exposure would increase further still under higher warming scenarios. These changes are likely to vary between
607 GCMs.

608
609 Due to the range in both absolute population numbers and the relative changes in population exposure between
610 present day, 1.5°C and 2°C across the four climate models in this event set, there is uncertainty in both how many
611 people might be exposed to a particular flood event, as well as how much this may change in the future. Moreover,
612 the range of present day absolute population numbers is often larger than the climate signal, which underlines the
613 difficulty in understanding current population exposure (Bates et al., 2021). This demonstrates the importance in
614 assessing a range of different climate model projections to understand the range of uncertainties, which taking an
615 event set approach enables because it allows many more realisations of a given event magnitude than is likely to
616 have occurred in the historical record to be considered. Overall, three of the four climate models utilized in this
617 study show that there is a difference in the percentage of the population exposed at a given return period under
618 1.5°C or 2°C climate change in comparison to present day. It is likely that the difference between 1.5°C and 2°C is
619 too small to determine a robust directional change above variability, particularly as only four of the >50 HAPPI
620 ensemble members are utilised in this analysis. Other studies have also shown a spread around the median in
621 precipitation, flood hazard and population exposure estimates under future scenarios (Bates et al., 2021; Swain et al.,
622 2020; Lopez-Cantu et al., 2020), as well as uncertain differences between 1.5°C and 2°C given the influence of
623 underlying uncertainty in the GCM and precipitation data (Uhe et al., 2019).

624

625 Other reasons for uncertainty in absolute population exposures likely stems from the choice of population data, and
626 the corresponding methodology used to assign population to pixels, as well as the underlying population data used to
627 inform the population totals. This is evidenced by the differences in total population between WorldPop, HRSL and
628 HRPDM as discussed in Section 2.3. Moreover, flood defences are not included in the model due to a lack of
629 available data, meaning the absolute population exposure numbers – particularly for the lower return periods where
630 flood defences are most likely to provide protection – will probably be an overestimate in some locations. If flood
631 defence information were available, the standards of protection could be applied to the exposure estimates provided
632 in this dataset to estimate population exposure when flood defences are included. On the other hand, as this study
633 does not include estimates of coastal flooding, the population exposure estimates may also be an underestimate. This
634 means that it is important to consider that the exposure estimates outlined in this study are for inland rainfall-driven
635 flooding only.

636 **4.4 Limitations of Event Set Size**

637 Population exposure estimates above the 30-year return period are subject to significant uncertainty due to the
638 limited number of samples (mean of <12.7 samples across the four climate models) available in the event set with
639 these return periods. As a result, the changes in population exposure between current, 1.5°C and 2°C above the 30-
640 year return period were not considered in this study. This was an acceptable trade off based on this current work, as
641 this study was most focused on understanding changes in lower magnitude, higher frequency events. Flood events
642 >30-year return period are often valley-filling, and therefore the impact of such events is already likely to be very
643 significant for the population, as demonstrated during Hurricane Maria (Pasch et al., 2018). Larger events also often
644 lead to a greater domestic and international response. However, smaller more frequent events lead to the erosion of
645 resilience in communities over time, and do not receive the same level of relief or response (Hamdan, 2015; Bull-
646 Kamanga et al., 2003; Allen et al., 2017; United Nations Office for Disaster Risk Reduction, 2019). Research to date
647 has also mostly focused on changes in the 100-year return period event (Arnell and Gosling, 2016; Lehner et al.,
648 2006; Hirabayashi et al., 2013). Therefore, assessing changes in lower magnitude, higher frequency events was a
649 key aim of this study. To detect changes in the 100-year return period population exposure, a much longer event set
650 would be required to detect a significant change between 1.5°C and 2°C. Although we have shown that 20 events
651 like Hurricane Maria do occur in the event set overall, preferably there would be at least 30-50 events to have
652 confidence in relative changes, as is shown in Figure 6. This would require at least 1000 years of synthetic data per
653 climate model as a minimum. This should be considered in the future when producing event sets derived from
654 GCMs with the intention to utilise these in flood impact modelling. Inevitably, running a much larger ensemble
655 comes at the expense of computational cost, therefore a trade-off, particularly with inundation model resolution, is
656 likely to be necessary.

657 **5 Conclusions**

658 We present the most detailed estimates of present day and future (1.5°C and 2°C) hurricane rainfall-driven flood
659 hazard and population exposure estimates in Puerto Rico to date. This analysis quantifies present day population

660 exposure to flooding in Puerto Rico for small to medium sized events (<30-year return period). Population exposure
661 to flooding is likely to increase under both 1.5°C and 2°C climate change. Estimates here suggest that for the present
662 day 8-10% of the total population of Puerto Rico would be exposed to flooding (defined as residing at a location
663 with inundation depth > 10cm) from hurricane rainfall every 5 years, increasing by 2-15% and 1-20% at 1.5°C and
664 2°C, respectively. Increases in the number of people exposed to small to medium sized flood events (<30-year return
665 period) could have a cumulative negative impact on the long-term resilience of the Puerto Rican population without
666 appropriate adaptation. Uncertainty in absolute population exposure estimates, as well as the range in estimated
667 percentage increases in flooding under 1.5°C and 2°C should be considered when using these estimates to inform
668 appropriate adaptation.

669
670 Through validation of our model in comparison with observed high water mark data for Hurricane Maria (~115-year
671 return period rainfall event), we find that our model is able to replicate similar levels of flooding to that which
672 occurred, and that there are events like Hurricane Maria in the event set when events with both similar maximum
673 total rainfall and spatial track characteristics are considered. This has important implications for future research, as
674 an event-based approach allows the assessment of many more plausible scenarios than is available in the observed
675 historical record.

676
677 Puerto Rico is predicted to experience increased population exposure to flooding associated with hurricane rainfall
678 in the future under 1.5°C and 2°C climate change. These findings add to the growing body of research that
679 highlights the critical and disproportionate risk climate change poses to Small Island Developing States, amidst the
680 uncomfortable irony that they have contributed amongst the least greenhouse gas emissions responsible for
681 anthropogenic climate change (Hoegh-Guldberg et al., 2018; Thomas et al., 2020). This highlights simultaneously
682 the impact of every increment of global temperature increase for Small Island Developing States and thus the
683 importance of high-ambition mitigation efforts, as well as the urgent need for increased climate change adaptation
684 and disaster risk reduction in the region.

685

686 **Data Availability**

687 The HAPPI climate model data described in Mitchell et al., (2017) <https://doi.org/10.5194/gmd-10-571-2017> can be
688 found and downloaded under a Attribution-NonCommercial-ShareAlike 2.0 Generic License at:

689 https://www.happimip.org/happi_data/

690 The LiDAR data can be found on the USGS Data Access Viewer:

691 <https://coast.noaa.gov/dataviewer/#/lidar/search/where:ID=8630>

692 The LISFLOOD-FP hydraulic engine is available to download at: LISFLOOD-FP Developers. (2020). LISFLOOD-
693 FP 8.0 hydrodynamic model (Version 8.0). [Software]. Zenodo. <https://doi.org/10.5281/zenodo.4073011>

694 The WorldPop population data can be found at: Bondarenko et al., (2020) doi:10.5258/SOTON/WP00684 under a
695 Creative Commons Attribution 4.0 International License.

696 The High Water Mark data can be found on the USGS Flood Event Viewer:
697 <https://stn.wim.usgs.gov/FEV/#MariaSeptember2017>
698 IMERG data can be downloaded from the Global Precipitation Measurement database at:
699 <https://gpm.nasa.gov/data/imerg>
700 NCEP Stage IV data can be downloaded at: Du, J. 2011. NCEP/EMC 4KM Gridded Data (GRIB) Stage IV Data.
701 Version 1.0. UCAR/NCAR - Earth Observing Laboratory. <https://doi.org/10.5065/D6PG1QDD>
702 The probability of inundation and corresponding population exposure estimates maps are available via the data.bris
703 Research Data Repository (doi available at final publication).
704 The probability of inundation (event set) flood hazard maps from Archer et al., (2023) are available via the
705 University of Bristol Research Data Repository (data.bris) at
706 <https://doi.org/10.5523/bris.2qtfnf5lw52u52snyl5ruwekef> under a Creative Commons "CC BY-NC 4.0" license.

707 **Author contribution**

708 LA conceptualized, conducted the analysis, methodology and validation and wrote the manuscript; JN and PDB
709 conceptualized, supervised and contributed to the analysis, methodology and validation; EV, DC and JS were
710 involved in the data curation and methodology; DM was involved in conceptualization. All authors were involved in
711 reviewing and editing the manuscript.

712

713 **Competing interests**

714 The authors declare that they have no conflict of interest.

715 **Acknowledgments**

716 Leanne Archer is supported by the UKRI NERC GW4+ Doctoral Training Partnership NE/S007504/1. Paul Bates is
717 supported by a Royal Society Wolfson Research Merit award. Jeffrey Neal is supported by UKRI NERC grants
718 NE/S003061/1 and NE/S006079/1. Emily Vosper is supported by the UKRI ERSPC Centre for Doctoral Training.
719

720 **References**

721 Aldridge, T., Gunawan, O., Moore, R. J., Cole, S. J., Boyce, G., and Cowling, R.: Developing an impact library for
722 forecasting surface water flood risk, *J Flood Risk Manag*, 13, <https://doi.org/10.1111/jfr3.12641>, 2020.
723 Allen, A., Zilbert Soto, L., Wesely, J., Belkow, T., Ferro, V., Lambert, R., Langdown, I., and Samanamú, A.: From
724 state agencies to ordinary citizens: reframing risk-mitigation investments and their impact to disrupt urban risk traps
725 in Lima, Peru, *Environ Urban*, 29, 477–502, <https://doi.org/10.1177/0956247817706061>, 2017.
726 Puerto Rico Probability of Flood Inundation Maps:
727 Arnell, N. W. and Gosling, S. N.: The impacts of climate change on river flood risk at the global scale, *Clim*
728 *Change*, 134, 387–401, <https://doi.org/10.1007/S10584-014-1084-5>, 2016.
729 Audi, C., Segarra, L., Irwin, C., Craig, P., Skelton, C., and Bestul, N.: Ascertainment of the Estimated Excess
730 Mortality from Hurricane María in Puerto Rico, Washington D.C., 2018.
731 Barnes, R.: Parallel non-divergent flow accumulation for trillion cell digital elevation models on desktops or
732 clusters, *Environmental Modelling & Software*, 92, 202–212, <https://doi.org/10.1016/J.ENVSOFT.2017.02.022>,
733 2017.

734 Bates, P. D., Horritt, M. S., and Fewtrell, T. J.: A simple inertial formulation of the shallow water equations for
735 efficient two-dimensional flood inundation modelling, *J Hydrol (Amst)*, 387, 33–45,
736 <https://doi.org/10.1016/j.jhydrol.2010.03.027>, 2010.

737 Bates, P. D., Quinn, N., Sampson, C., Smith, A., Wing, O., Sosa, J., Savage, J., Olcese, G., Neal, J., Schumann, G.,
738 Giustarini, L., Coxon, G., Porter, J. R., Amodeo, M. F., Chu, Z., Lewis-Gruss, S., Freeman, N. B., Houser, T.,
739 Delgado, M., Hamidi, A., Bolliger, I., McCusker, K., Emanuel, K., Ferreira, C. M., Khalid, A., Haigh, I. D.,
740 Couasnon, A., Kopp, R., Hsiang, S., and Krajewski, W. F.: Combined modelling of US fluvial, pluvial and coastal
741 flood hazard under current and future climates, *Water Resour Res*, 57, <https://doi.org/10.1029/2020wr028673>, 2021.

742 Bates, P. D., Savage, J., Wing, O., Quinn, N., Sampson, C., Neal, J., and Smith, A.: A climate-conditioned
743 catastrophe risk model for UK flooding, *Natural Hazards and Earth System Sciences*, 23, 891–908,
744 <https://doi.org/10.5194/NHESS-23-891-2023>, 2023.

745 Bentsen, M., Bethke, I., Debernard, J. B., Iversen, T., Kirkevåg, A., Seland, Ø., Drange, H., Roelandt, C., Seierstad,
746 I. A., Hoose, C., and Kristjánsson, J. E.: The Norwegian Earth System Model, NorESM1-M – Part 1: Description
747 and basic evaluation of the physical climate, *Geosci Model Dev*, 6, 687–720, [https://doi.org/10.5194/GMD-6-687-](https://doi.org/10.5194/GMD-6-687-2013)
748 2013, 2013.

749 Bernet, D. B., Zischg, A. P., Prasuhn, V., and Weingartner, R.: Modeling the extent of surface water floods in rural
750 areas: Lessons learned from the application of various uncalibrated models, *Environmental Modelling and Software*,
751 109, 134–151, <https://doi.org/10.1016/j.envsoft.2018.08.005>, 2018.

752 Bernet, D. B., Trefalt, S., Martius, O., Weingartner, R., Mosimann, M., Röthlisberger, V., and Zischg, A. P.:
753 Characterizing precipitation events leading to surface water flood damage over large regions of complex terrain,
754 *Environmental Research Letters*, 14, <https://doi.org/10.1088/1748-9326/ab127c>, 2019.

755 Bessette-Kirton, E. K., Coe, J. A., Schulz, W. H., Cerovski-Darriau, C., and Einbund, M. M.: Mobility
756 characteristics of debris slides and flows triggered by Hurricane Maria in Puerto Rico, *Landslides*, 17, 2795–2809,
757 <https://doi.org/10.1007/s10346-020-01445-z>, 2020.

758 Blanc, J., Hall, J. W., Roche, N., Dawson, R. J., Cesses, Y., Burton, A., and Kilsby, C. G.: Enhanced efficiency of
759 pluvial flood risk estimation in urban areas using spatial-temporal rainfall simulations, *J Flood Risk Manag*, 5, 143–
760 152, <https://doi.org/10.1111/j.1753-318X.2012.01135.x>, 2012.

761 Mapping the world to help aid workers, with weakly, semi-supervised learning:
762 <https://ai.facebook.com/blog/mapping-the-world-to-help-aid-workers-with-weakly-semi-supervised-learning>, last
763 access: 1 June 2020.

764 Bondarenko, M., Kerr, D., Sorichetta, A., and Tatem, A. J.: Census/projection-disaggregated gridded population
765 datasets for 189 countries in 2020 using Built-Settlement Growth Model (BSGM) outputs, WorldPop, University of
766 Southampton, Southampton, <https://doi.org/10.5258/SOTON/WP00684>, 2020.

767 Bull-Kamanga, L., Diagne, K., Lavell, A., Leon, E., Lerise, F., MacGregor, H., Maskrey, A., Meshack, M., Pelling,
768 M., Reid, H., Satterthwaite, D., Songsore, J., Westgate, K., and Yitambe, A.: From everyday hazards to disasters: the
769 accumulation of risk in urban areas, *Environ Urban*, 15, 193–204, <https://doi.org/10.1177/095624780301500109>,
770 2003.

771 Burgess, C. P., Taylor, M. A., Stephenson, T., Mandal, A., and Powell, L.: A macro-scale flood risk model for
772 Jamaica with impact of climate variability, *Natural Hazards*, 78, 231–256, [https://doi.org/10.1007/s11069-015-1712-](https://doi.org/10.1007/s11069-015-1712-z)
773 z, 2015.

774 Caban, P.: Hurricane Maria’s Aftermath: Redefining Puerto Rico’s Colonial Status, *Current History*, 118, 43–49,
775 2019.

776 Czajkowski, J., Villarini, G., Montgomery, M., Michel-Kerjan, E., and Goska, R.: Assessing Current and Future
777 Freshwater Flood Risk from North Atlantic Tropical Cyclones via Insurance Claims, *Sci Rep*, 7, 1–10,
778 <https://doi.org/10.1038/srep41609>, 2017.

779 Daron, J., Lorenz, S., Taylor, A., and Dessai, S.: Communicating future climate projections of precipitation change,
780 *Clim Change*, 166, 1–20, <https://doi.org/10.1007/S10584-021-03118-9/FIGURES/5>, 2021.

781 Dinku, T., Chidzambwa, S., Ceccato, P., Connor, S. J., and Ropelewski, C. F.: Validation of high-resolution satellite
782 rainfall products over complex terrain, <http://dx.doi.org/10.1080/01431160701772526>, 29, 4097–4110,
783 <https://doi.org/10.1080/01431160701772526>, 2008.

784 NCEP/EMC 4KM Gridded Data (GRIB) Stage IV Data:
785 Emanuel, K. and Jagger, T.: On Estimating Hurricane Return Periods, *J Appl Meteorol Climatol*, 49, 837–844,
786 <https://doi.org/10.1175/2009JAMC2236.1>, 2010.

787 Emanuel, K., DesAutels, C., Holloway, C., and Korty, R.: Environmental Control of Tropical Cyclone Intensity, *J*
788 *Atmos Sci*, 61, 843–858, [https://doi.org/10.1175/1520-0469\(2004\)061<0843:ECOTCI>2.0.CO;2](https://doi.org/10.1175/1520-0469(2004)061<0843:ECOTCI>2.0.CO;2), 2004.

789 Emanuel, K., Sundararajan, R., and Williams, J.: Hurricanes and Global Warming: Results from Downscaling IPCC
790 AR4 Simulations, *Bull Am Meteorol Soc*, 89, 347–368, <https://doi.org/10.1175/BAMS-89-3-347>, 2008.

791 Falconer, R. H., Cobby, D., Smyth, P., Astle, G., Dent, J., and Golding, B.: Pluvial flooding: new approaches in
792 flood warning, mapping and risk management, *J Flood Risk Manag*, 2, 198–208, <https://doi.org/10.1111/j.1753-318X.2009.01034.x>, 2009.

793 Feldmann, M., Emanuel, K., Zhu, L., and Lohmann, U.: Estimation of Atlantic Tropical Cyclone Rainfall Frequency
794 in the United States, *J Appl Meteorol Climatol*, 58, 1853–1866, <https://doi.org/10.1175/JAMC-D-19-0011.1>, 2019.

795 Freitas, E. da S., Coelho, V. H. R., Xuan, Y., Melo, D. de C. D., Gadelha, A. N., Santos, E. A., Galvão, C. de O.,
796 Ramos Filho, G. M., Barbosa, L. R., Huffman, G. J., Petersen, W. A., and Almeida, C. das N.: The performance of
797 the IMERG satellite-based product in identifying sub-daily rainfall events and their properties, *J Hydrol (Amst)*,
798 589, 125128, <https://doi.org/10.1016/J.JHYDROL.2020.125128>, 2020.

799 Gao, S., Zhang, J., Li, D., Jiang, H., and Fang, Z. N.: Evaluation of Multiradar Multisensor and Stage IV
800 Quantitative Precipitation Estimates during Hurricane Harvey, *Nat Hazards Rev*, 22, 04020057,
801 [https://doi.org/10.1061/\(ASCE\)NH.1527-6996.0000435](https://doi.org/10.1061/(ASCE)NH.1527-6996.0000435), 2020.

802 Guerreiro, S. B., Glenis, V., Dawson, R. J., and Kilsby, C.: Pluvial flooding in European cities-A continental
803 approach to urban flood modelling, *Water (Switzerland)*, 9, <https://doi.org/10.3390/w9040296>, 2017.

804 Habib, E., Larson, B. F., and Grascel, J.: Validation of NEXRAD multisensor precipitation estimates using an
805 experimental dense rain gauge network in south Louisiana, *J Hydrol (Amst)*, 373, 463–478,
806 <https://doi.org/10.1016/J.JHYDROL.2009.05.010>, 2009.

807 Hall, J.: Direct Rainfall Flood Modelling: The Good, the Bad and the Ugly, *Australasian Journal of Water
808 Resources*, 19, 74–85, <https://doi.org/10.7158/13241583.2015.11465458>, 2015.

809 Hamdan, F.: Intensive and extensive disaster risk drivers and interactions with recent trends in the global political
810 economy, with special emphasis on rentier states, *International Journal of Disaster Risk Reduction*, 14, 273–289,
811 <https://doi.org/10.1016/j.ijdrr.2014.09.004>, 2015.

812 Hankin, B., Waller, S., Astle, G., and Kellagher, R.: Mapping space for water: screening for urban flash flooding, *J
813 Flood Risk Manag*, 1, 13–22, <https://doi.org/10.1111/j.1753-318x.2008.00003.x>, 2008.

814 Hawker, L., Bates, P., Neal, J., and Rougier, J.: Perspectives on Digital Elevation Model (DEM) Simulation for
815 Flood Modeling in the Absence of a High-Accuracy Open Access Global DEM, *Front Earth Sci (Lausanne)*, 6,
816 <https://doi.org/10.3389/feart.2018.00233>, 2018.

817 Hernández Ayala, J. J. and Matyas, C. J.: Tropical cyclone rainfall over Puerto Rico and its relations to
818 environmental and storm-specific factors, *International Journal of Climatology*, 36, 2223–2237,
819 <https://doi.org/10.1002/joc.4490>, 2016.

820 Hernández Ayala, J. J., Keellings, D., Waylen, P. R., and Matyas, C. J.: Extreme floods and their relationship with
821 tropical cyclones in Puerto Rico, *Hydrological Sciences Journal*, 62, 2103–2119,
822 <https://doi.org/10.1080/02626667.2017.1368521>, 2017.

823 Hirabayashi, Y., Mahendran, R., Koirala, S., Konoshima, L., Yamazaki, D., Watanabe, S., Kim, H., and Kanae, S.:
824 Global flood risk under climate change, *Nat Clim Chang*, 3, 816–821, <https://doi.org/10.1038/nclimate1911>, 2013.

825 Hoegh-Guldberg, O., Jacob, D., Taylor, M., Bindi, M., Brown, S., Camilloni, I., Diedhiou, A., and Djalante, R.:
826 Chapter 3: Impacts of 1.5°C global warming on natural and human systems, in: *Global warming of 1.5°C. An IPCC
827 Special Report on the impacts of global warming of 1.5°C above pre-industrial levels and related global greenhouse
828 gas emission pathways, in the context of strengthening the global response to the threat of climate change, edited by:
829 Intergovernmental Panel on Climate Change, Intergovernmental Panel on Climate Change, Geneva, 175–311, 2018.*

830 Hughes, K. S. and Schulz, W. H.: Map Depicting Susceptibility to Landslides Triggered by Intense Rainfall. Open-
831 File Report 2020–1022, Denver, <https://doi.org/https://doi.org/10.3133/ofr20201022>, 2020.

832 IPCC: Summary for Policymakers, in: *Global Warming of 1.5°C. An IPCC Special Report on the impacts of global
833 warming of 1.5°C above pre-industrial levels and related global greenhouse gas emission pathways, in the context of
834 strengthening the global response to the threat of climate change, edited by: Masson-Delmotte, V., Zhai, P., Pörtner,
835 H.-O., Roberts, D., Skea, J., Shukla, P. R., Pirani, A., Moufouma-Okia, W., Péan, C., Pidcock, R., Connors, S.,
836 Matthews, J. B. R., Chen, Y., Zhou, X., Gomis, M. I., Lonnoy, E., Maycock, T., Tignor, M., and Waterfield, T.,
837 Cambridge University Press, Cambridge, 1–24, 2018.*

838 IPCC: Summary for Policymakers, in: *Climate Change 2021: The Physical Science Basis. Contribution of Working
839 Group I to the Sixth Assessment Report of the Intergovernmental Panel on Climate Change, edited by: Masson-
840 Delmotte, V., Zhai, P., Pirani, A., Connors, S. L., Péan, C., Berger, S., Caud, N., Chen, Y., Goldfarb, L., Gomis, M.
841 I., Huang, M., Leitzell, K., Lonnoy, E., Matthews, J. B. R., Maycock, T. K., Waterfield, T., Yelekçi, O., Yu, R., and
842 Zhou, B., Cambridge University Press, Cambridge, 2021.*

844 Iversen, T., Bentsen, M., Bethke, I., Debernard, J. B., Kirkevåg, A., Seland, Ø., Drange, H., Kristjansson, J. E.,
845 Medhaug, I., Sand, M., and Seierstad, I. A.: The Norwegian Earth System Model, NorESM1-M – Part 2: Climate
846 response and scenario projections, *Geosci Model Dev*, 6, 389–415, <https://doi.org/10.5194/GMD-6-389-2013>, 2013.
847 Jetten, V.: CHaRIM Project St Vincent National Flood Hazard Map Methodology and Validation Report, Enschede,
848 The Netherlands, 2016.

849 Jiménez Cisneros, B. E., Oki, T., Arnell, N. W., Benito, G., Cogley, J. G., Döll, P., Jiang, T., and Mwakalila, S. S.:
850 Freshwater Resources, in: *Climate Change 2014: Impacts, Adaptation, and Vulnerability. Part A: Global and Sectoral*
851 *Aspects. Contribution of Working Group II to the Fifth Assessment Report of the Intergovernmental Panel on*
852 *Climate Change*, edited by: Field, C. B., Barros, V. R., Dokken, D. J., Mach, K. J., Mastrandrea, M. D., Bilir, T. E.,
853 Chatterjee, M., Ebi, K. L., Estrada, Y. O., Genova, R. C., Girma, B., Kissel, E. S., Levy, A. N., MacCracken, S.,
854 Mastrandrea, P. R., and L.L.White, Cambridge University Press, Cambridge, 2014.

855 Joyette, A. R. T., Nurse, L. A., and Pulwarty, R. S.: Disaster risk insurance and catastrophe models in risk-prone
856 small Caribbean islands, *Disasters*, 39, 467–492, <https://doi.org/10.1111/disa.12118>, 2014.

857 Keellings, D. and Hernández Ayala, J. J.: Extreme Rainfall Associated With Hurricane Maria Over Puerto Rico and
858 Its Connections to Climate Variability and Change, *Geophys Res Lett*, 46, 2964–2973,
859 <https://doi.org/10.1029/2019GL082077>, 2019.

860 Kirkevåg, A., Iversen, T., Seland, Ø., Hoose, C., Kristjánsson, J. E., Struthers, H., Ekman, A. M. L., Ghan, S.,
861 Griesfeller, J., Nilsson, E. D., and Schulz, M.: Aerosol–climate interactions in the Norwegian Earth System Model –
862 NorESM1-M, *Geosci Model Dev*, 6, 207–244, <https://doi.org/10.5194/GMD-6-207-2013>, 2013.

863 Knutson, T., Camargo, S. J., Chan, J. C. L., Emanuel, K., Ho, C.-H., Kossin, J., Mohapatra, M., Satoh, M., Sugi, M.,
864 Walsh, K., and Wu, L.: Tropical Cyclones and Climate Change Assessment: Part II. Projected Response to
865 Anthropogenic Warming, *Bull Am Meteorol Soc*, 101, E303–E322, <https://doi.org/10.1175/bams-d-18-0194.1>,
866 2020.

867 Kossin, J. P., Knapp, K. R., Olander, T. L., and Velden, C. S.: Global increase in major tropical cyclone exceedance
868 probability over the past four decades, *Proceedings of the National Academy of Sciences*, 117, 11975–11980,
869 <https://doi.org/10.1073/PNAS.1920849117>, 2020.

870 Lehner, B., Döll, P., Alcamo, J., Henrichs, T., and Kaspar, F.: Estimating the Impact of Global Change on Flood and
871 Drought Risks in Europe: A Continental, Integrated Analysis, *Clim Change*, 75, 273–299,
872 <https://doi.org/10.1007/S10584-006-6338-4>, 2006.

873 Leopold, L. B. and Maddock, T.: *The Hydraulic Geometry of Stream Channels and Some Physiographic*
874 *Implications*, Washington D.C., 1953.

875 Leyk, S., Gaughan, A. E., Adamo, S. B., De Sherbinin, A., Balk, D., Freire, S., Rose, A., Stevens, F. R.,
876 Blankespoor, B., Frye, C., Comenetz, J., Sorichetta, A., Macmanus, K., Pistolesi, L., Levy, M., Tatem, A. J., and
877 Pesaresi, M.: The spatial allocation of population: a review of large-scale gridded population data products and their
878 fitness for use, *Earth Syst Sci Data*, 11, 1385–1409, <https://doi.org/10.5194/essd-11-1385-2019>, 2019.

879 Li, Z., Tang, G., Kirstetter, P., Gao, S., Li, J. L. F., Wen, Y., and Hong, Y.: Evaluation of GPM IMERG and its
880 constellations in extreme events over the conterminous united states, *J Hydrol (Amst)*, 606, 127357,
881 <https://doi.org/10.1016/J.JHYDROL.2021.127357>, 2022.

882 LISFLOOD-FP Developers: LISFLOOD-FP 8.0 hydrodynamic model (8.0),
883 <https://doi.org/https://doi.org/10.5281/zenodo.4073011>, 2020.

884 Lloyd, C. T., Sorichetta, A., and Tatem, A. J.: High resolution global gridded data for use in population studies, *Sci*
885 *Data*, 4, 1–17, <https://doi.org/10.1038/sdata.2017.1>, 2017.

886 Lopez-Cantu, T., Prein, A. F., and Samaras, C.: Uncertainties in Future U.S. Extreme Precipitation From
887 Downscaled Climate Projections, *Geophys Res Lett*, 47, <https://doi.org/10.1029/2019GL086797>, 2020.

888 Lu, P., Lin, N., Emanuel, K., Chavas, D., and Smith, J.: Assessing Hurricane Rainfall Mechanisms Using a Physics-
889 Based Model: Hurricanes Isabel (2003) and Irene (2011), *Journal of Atmospheric Sciences*, 75, 2337–2358,
890 <https://doi.org/10.1175/JAS-D-17-0264.1>, 2018.

891 Lumbroso, D., Boyce, S., Bast, H., and Walmsley, N.: The challenges of developing rainfall intensity-duration-
892 frequency curves and national flood hazard maps for the Caribbean, *The Journal of Flood Risk Management*, 4, 42–
893 52, 2011.

894 Main, J. A., Dillard, M., Kuligowski, E. D., Davis, B., Dukes, J., Harrison, K., Helgeson, J., Johnson, K., Levitan,
895 M., Mitrani-Reiser, J., Weaver, S., Yeo, D., Aponte-Bermúdez, L. D., Cline, J., Kirsch, T., and Ross, W. L.:
896 Learning from Hurricane Maria’s Impacts on Puerto Rico: A Progress Report, Washington D.C.,
897 <https://doi.org/10.6028/NIST.SP.1262>, 2021.

898 Marks, D. G.: The beta and advection model for hurricane track forecasting: NOAA Tech. Memo, NWS NMC 70,
899 Camp Springs, 1992.

900 Mazza, E. and Chen, S. S.: Tropical Cyclone Rainfall Climatology, Extremes, and Flooding Potential from Remote
901 Sensing and Reanalysis Datasets over the Continental United States, *J Hydrometeorol*, 24, 1549–1562,
902 <https://doi.org/10.1175/JHM-D-22-0199.1>, 2023.

903 Mazzoleni, M., Mård, J., Rusca, M., Odongo, V., Lindersson, S., and Di Baldassarre, G.: Floodplains in the
904 Anthropocene: A global analysis of the interplay between human population, built environment and flood severity,
905 *Water Resour Res*, <https://doi.org/10.1029/2020WR027744>, 2020.

906 Mei, W. and Xie, S.-P.: Intensification of landfalling typhoons over the northwest Pacific since the late 1970s,
907 *Nature Geoscience* 2016 9:10, 9, 753–757, <https://doi.org/10.1038/ngeo2792>, 2016.

908 Michaud, J. and Kates, J.: Public Health in Puerto Rico after Hurricane Maria, San Francisco, 2017.

909 Mitchell, D., James, R., Forster, P. M., Betts, R. A., Shiogama, H., and Allen, M.: Realizing the impacts of a 1.5 °C
910 warmer world, *Nat Clim Chang*, 6, 735–737, <https://doi.org/10.1186/s40665-015-0010-z>, 2016.

911 Mitchell, D., Achutarao, K., Allen, M., Bethke, I., Beyerle, U., Ciavarella, A., Forster, P. M., Fuglestedt, J., Gillett,
912 N., Haustein, K., Ingram, W., Iversen, T., Kharin, V., Klingaman, N., Massey, N., Fischer, E., Schleussner, C.-F.,
913 Scinocca, J., Seland, Ø., Shiogama, H., Shuckburgh, E., Sparrow, S., Stone, D., Uhe, P., Wallom, D., Wehner, M.,
914 and Zaaboul, R.: Half a degree additional warming, prognosis and projected impacts (HAPPI): background and
915 experimental design, *Geosci. Model Dev*, 10, 571–583, <https://doi.org/10.5194/gmd-10-571-2017>, 2017.

916 Moftakhari, H. R., AghaKouchak, A., Sanders, B. F., and Matthew, R. A.: Cumulative hazard: The case of nuisance
917 flooding, *Earths Future*, 5, 214–223, <https://doi.org/10.1002/2016EF000494>, 2016.

918 Monioudi, I., Asariotis, R., Becker, A., Bhat, C., Dowding-Gooden, D., Esteban, M., Feyen, L., Mentaschi, L.,
919 Nikolaou, A., Nurse, L., Phillips, W., Smith, D., Satoh, M., Trotz, U. O., Velegrakis, A. F., Voukouvalas, E.,
920 Vousdoukas, M. I., and Witkop, R.: Climate change impacts on critical international transportation assets of
921 Caribbean Small Island Developing States (SIDS): the case of Jamaica and Saint Lucia, *Reg Environ Change*, 18,
922 2211–2225, <https://doi.org/10.1007/s10113-018-1360-4>, 2018.

923 Mycoo, M. A.: Beyond 1.5°C: vulnerabilities and adaptation strategies for Caribbean Small Island Developing
924 States, *Reg Environ Change*, 18, 2341–2353, <https://doi.org/10.1007/s10113-017-1248-8>, 2018.

925 Mycoo, M. A., Wairiu, M., Campbell, D., Duvat, V., Golbuu, Y., Maharaj, S., Nalau, J., Nunn, P., Pinnegar, J., and
926 Warrick, O.: Small Islands, in: *Climate Change 2022: Impacts, Adaptation and Vulnerability. Contribution of*
927 *Working Group II to the Sixth Assessment Report of the Intergovernmental Panel on Climate Change*, Cambridge
928 University Press, Cambridge, 2022.

929 IMERG: Integrated Multi-satellitE Retrievals for GPM | NASA Global Precipitation Measurement Mission:
930 <https://gpm.nasa.gov/data/imerg>, last access: 17 May 2023.

931 Major Hurricane Maria - September 20, 2017:

932 Neal, J., Schumann, G., and Bates, P.: A subgrid channel model for simulating river hydraulics and floodplain
933 inundation over large and data sparse areas, *Water Resour Res*, 48, <https://doi.org/10.1029/2012WR012514>, 2012.

934 Neal, J., Hawker, L., Savage, J., Durand, M., Bates, P., and Sampson, C.: Estimating River Channel Bathymetry in
935 Large Scale Flood Inundation Models, *Water Resour Res*, 57, <https://doi.org/10.1029/2020wr028301>, 2021.

936 Neal, J. C., Bates, P. D., Fewtrell, T. J., Hunter, N. M., Wilson, M. D., and Horritt, M. S.: Distributed whole city
937 water level measurements from the Carlisle 2005 urban flood event and comparison with hydraulic model
938 simulations, *J Hydrol (Amst)*, 368, 42–55, <https://doi.org/10.1016/j.jhydrol.2009.01.026>, 2009.

939 Nelson, B. R., Prat, O. P., Seo, D. J., and Habib, E.: Assessment and Implications of NCEP Stage IV Quantitative
940 Precipitation Estimates for Product Intercomparisons, *Weather Forecast*, 31, 371–394, <https://doi.org/10.1175/WAF-D-14-00112.1>, 2016.

942 Nicholls, R. J., Brown, S., Goodwin, P., Wahl, T., Lowe, J., Solan, M., Godbold, J. A., Haigh, I. D., Lincke, D.,
943 Hinkel, J., Wolf, C., and Merkens, J. L.: Stabilization of global temperature at 1.5°C and 2.0°C: Implications for
944 coastal areas, *Philosophical Transactions of the Royal Society A: Mathematical, Physical and Engineering Sciences*,
945 376, <https://doi.org/10.1098/rsta.2016.0448>, 2018.

946 Nurse, L. A., McLean, R. F., Agard Trinidad, J., Pascal Briguglio, L., Duvat-Magnan, V., Pelesikoti, N., Tompkins,
947 E., and Webb, A.: Small Islands, in: *Climate Change 2014: Impacts, Adaptation, and Vulnerability. Part B: Regional*
948 *Aspects. Contribution of Working Group II to the Fifth Assessment Report of the Intergovernmental Panel on*
949 *Climate Change*, edited by: Intergovernmental Panel on Climate Change, Cambridge, 1613–1654, 2014.

950 Nuswantoro, R., Diermanse, F., and Molkenhain, F.: Probabilistic flood hazard maps for Jakarta derived from a
951 stochastic rain-storm generator, *J Flood Risk Manag*, 9, 105–124, <https://doi.org/10.1111/jfr3.12114>, 2016.

952 Omranian, E., Sharif, H. O., and Tavakoly, A. A.: How Well Can Global Precipitation Measurement (GPM) Capture
953 Hurricanes? Case Study: Hurricane Harvey, *Remote Sensing* 2018, Vol. 10, Page 1150, 10, 1150,
954 <https://doi.org/10.3390/RS10071150>, 2018.

955 Ourbak, T. and Magnan, A. K.: The Paris Agreement and climate change negotiations: Small Islands, big players,
956 <https://doi.org/10.1007/s10113-017-1247-9>, 1 December 2018.

957 Pasch, R. J., Penny, A. B., and Berg, R.: Hurricane Maria 16–30 September 2017, National Hurricane Center
958 Tropical Cyclone Report, National Hurricane Center, Miami, 2018.

959 Patricola, C. M. and Wehner, M. F.: Anthropogenic influences on major tropical cyclone events, *Nature*, 563, 339–
960 346, <https://doi.org/10.1038/s41586-018-0673-2>, 2018.

961 Pickup, G. and Warner, R. F.: Effects of hydrologic regime on magnitude and frequency of dominant discharge, *J*
962 *Hydrol (Amst)*, 29, 51–75, [https://doi.org/10.1016/0022-1694\(76\)90005-6](https://doi.org/10.1016/0022-1694(76)90005-6), 1976.

963 Pokhrel, R., Cos, S. del, Montoya Rincon, J. P., Glenn, E., and González, J. E.: Observation and modeling of
964 Hurricane Maria for damage assessment, *Weather Clim Extrem*, 33, 100331,
965 <https://doi.org/10.1016/J.WACE.2021.100331>, 2021.

966 Pradhan, R. K., Markonis, Y., Vargas Godoy, M. R., Villalba-Pradas, A., Andreadis, K. M., Nikolopoulos, E. I.,
967 Papalexiou, S. M., Rahim, A., Tapiador, F. J., and Hanel, M.: Review of GPM IMERG performance: A global
968 perspective, *Remote Sens Environ*, 268, 112754, <https://doi.org/10.1016/J.RSE.2021.112754>, 2022.

969 Prat, O. P. and Nelson, B. R.: Evaluation of precipitation estimates over CONUS derived from satellite, radar, and
970 rain gauge data sets at daily to annual scales (2002–2012), *Hydrol. Earth Syst. Sci*, 19, 2037–2056,
971 <https://doi.org/10.5194/hess-19-2037-2015>, 2015.

972 Pratomy, R. A., Jetten, V., and Alkema, D.: Rural Flash-flood Behavior in Gouyave Watershed, Grenada,
973 Caribbean Island, *Geoplanning: Journal of Geomatics and Planning*, 3, 161,
974 <https://doi.org/10.14710/geoplanning.3.2.161-170>, 2016.

975 Ramos-Scharrón, C. E. and Arima, E.: Hurricane María’s Precipitation Signature in Puerto Rico: A Conceivable
976 Presage of Rains to Come, *Sci Rep*, 9, <https://doi.org/10.1038/s41598-019-52198-2>, 2019.

977 Ranasinghe, R., Ruane, A. C., Vautard, R., Arnell, N., Coppola, E., Cruz, F. A., Dessai, S., Islam, A. S., Rahimi, M.,
978 Ruiz, D., Carrascal, Sillmann, J., Sylla, M. B., Tebaldi, C., Wang, W., and Zaaboul, R.: Climate Change Information
979 for Regional Impact and for Risk Assessment, in: *Climate Change 2021: The Physical Science Basis. Contribution*
980 *of Working Group I to the Sixth Assessment Report of the Intergovernmental Panel on Climate Change*, edited
981 by: Masson-Delmotte, V., Zhai, P., Pirani, A., Connors, S. L., Péan, C., Berger, S., Caud, N., Chen, Y., Goldfarb, L.,
982 Gomis, M. I., Huang, M., Leitzell, K., Lonnoy, E., Matthews, J. B. R., Maycock, T. K., Waterfield, T., Yelekçi, O.,
983 Yu, R., and Zhou, B., Cambridge University Press, Cambridge, 2021.

984 Rappaport, E. N.: Fatalities in the United States from Atlantic Tropical Cyclones: New Data and Interpretation, *Bull*
985 *Am Meteorol Soc*, 95, 341–346, <https://doi.org/10.1175/BAMS-D-12-00074.1>, 2014.

986 Rasmussen, D. J., Bittermann, K., Buchanan, M. K., Kulp, S., Strauss, B. H., Kopp, R. E., and Oppenheimer, M.:
987 Extreme sea level implications of 1.5 °C, 2.0 °C, and 2.5 °C temperature stabilization targets in the 21st and 22nd
988 centuries, *Environmental Research Letters*, 13, 034040, <https://doi.org/10.1088/1748-9326/AAAC87>, 2018.

989 Reed, F., Gaughan, A., Stevens, F., Yetman, G., Sorichetta, A., and Tatem, A.: Gridded Population Maps Informed
990 by Different Built Settlement Products, *Data (Basel)*, 3, 33, <https://doi.org/10.3390/data3030033>, 2018.

991 Rios Gaona, M. F., Overeem, A., Brasjen, A. M., Meirink, J. F., Leijnse, H., and Uijlenhoet, R.: Evaluation of
992 Rainfall Products Derived from Satellites and Microwave Links for the Netherlands, *IEEE Transactions on*
993 *Geoscience and Remote Sensing*, 55, 6849–6859, <https://doi.org/10.1109/TGRS.2017.2735439>, 2017.

994 Rios Gaona, M. F., Villarini, G., Zhang, W., and Vecchi, G. A.: The added value of IMERG in characterizing
995 rainfall in tropical cyclones, *Atmos Res*, 209, 95–102, <https://doi.org/10.1016/J.ATMOSRES.2018.03.008>, 2018.

996 Rivera, D. Z.: Disaster Colonialism: A Commentary on Disasters beyond Singular Events to Structural Violence, *Int*
997 *J Urban Reg Res*, <https://doi.org/10.1111/1468-2427.12950>, 2020.

998 Rosenzweig, B. R., McPhillips, L., Chang, H., Cheng, C., Welty, C., Matsler, M., Iwaniec, D., and Davidson, C. I.:
999 Pluvial flood risk and opportunities for resilience, *WIREs Water*, 5, <https://doi.org/10.1002/wat2.1302>, 2018.

1000 Rözer, V., Kreibich, H., Schröter, K., Müller, M., Sairam, N., Doss-Gollin, J., Lall, U., and Merz, B.: Probabilistic
1001 Models Significantly Reduce Uncertainty in Hurricane Harvey Pluvial Flood Loss Estimates, *Earths Future*, 7, 384–
1002 394, <https://doi.org/10.1029/2018EF001074>, 2019.

1003 Von Salzen, K., Scinocca, J. F., McFarlane, N. A., Li, J., Cole, J. N. S., Plummer, D., Versegny, D., Reader, M. C.,
1004 Ma, X., Lazare, M., and Solheim, L.: The Canadian Fourth Generation Atmospheric Global Climate Model
1005 (CanAM4). Part I: Representation of Physical Processes, *Atmosphere-Ocean*, 51, 104–125,
1006 <https://doi.org/10.1080/07055900.2012.755610>, 2013.

1007 Sampson, C. C., Bates, P. D., Neal, J. C., and Horritt, M. S.: An automated routing methodology to enable direct
1008 rainfall in high resolution shallow water models, *Hydrol Process*, 27, 467–476, <https://doi.org/10.1002/hyp.9515>,
1009 2013.

1010 Sampson, C. C., Smith, A. M., Bates, P. B., Neal, J. C., Alfieri, L., and Freer, J. E.: A high-resolution global flood
1011 hazard model, *Water Resour Res*, 51, 7358–7381, <https://doi.org/10.1002/2015WR016954>, 2015.

1012 Savage, J. T. S., Bates, P., Freer, J., Neal, J., and Aronica, G.: When does spatial resolution become spurious in
1013 probabilistic flood inundation predictions?, *Hydrol Process*, 30, 2014–2032, <https://doi.org/10.1002/hyp.10749>,
1014 2016.

1015 Sayers, P. B., Horritt, M. S., Carr, S., Kay, A., Mauz, J., Lamb, R., and Penning-Rowsell, E.: Third UK Climate
1016 Change Risk Assessment (CCRA3) Future flood risk Main Report Final Report prepared for the Committee on
1017 Climate Change, UK, London, 2020.

1018 Schaller, N., Sillmann, J., Müller, M., Haarsma, R., Hazeleger, W., Hegdahl, T. J., Kelder, T., van den Oord, G.,
1019 Weerts, A., and Whan, K.: The role of spatial and temporal model resolution in a flood event storyline approach in
1020 western Norway, *Weather Clim Extrem*, 29, <https://doi.org/10.1016/J.WACE.2020.100259>, 2020.

1021 Seneviratne, S. I., Zhang, X., Adnan, M., Badi, W., Dereczynski, C., Luca, A. Di, Ghosh, S., Iskandar, I., Kossin, J.,
1022 Lewis, S., Otto, F., Pinto, I., Satoh, M., Vicente-Serrano, S. M., Wehner, M., and B. Zhou: Weather and Climate
1023 Extreme Events in a Changing Climate, in: *Climate Change 2021: The Physical Science Basis. Contribution of*
1024 *Working Group I to the Sixth Assessment Report of the Intergovernmental Panel on Climate Change*, edited by:
1025 Masson-Delmotte, V., Zhai, P., Pirani, A., Connors, S. L., Péan, C., Berger, S., Caud, N., Chen, Y., Goldfarb, L.,
1026 Gomis, M. I., Huang, M., Leitzell, K., Lonnoy, E., Matthews, J. B. R., Maycock, T. K., T. Waterfield, Yelekçi, O.,
1027 Yu, R., and Zhou, B., Cambridge University Press, Cambridge, 2021.

1028 Simley, J. D. and Carswell Jr, W. J.: The National Map-Hydrography Using the Data: Fact Sheet 2009-3054, 2010.

1029 Skougaard Kaspersen, P., Høegh Ravn, N., Arnbjerg-Nielsen, K., Madsen, H., and Drews, M.: Comparison of the
1030 impacts of urban development and climate change on exposing European cities to pluvial flooding, *Hydrol Earth*
1031 *Syst Sci*, 21, 4131–4147, <https://doi.org/10.5194/HESS-21-4131-2017>, 2017.

1032 Smith, A., Bates, P. D., Wing, O., Sampson, C., Quinn, N., and Neal, J.: New estimates of flood exposure in
1033 developing countries using high-resolution population data, *Nat Commun*, 10, 1814, [https://doi.org/10.1038/s41467-](https://doi.org/10.1038/s41467-019-09282-y)
1034 [019-09282-y](https://doi.org/10.1038/s41467-019-09282-y), 2019.

1035 Smith, J. A., Sturdevant-Rees, Paula., Baeck, M. Lynn., and Larsen, M. C.: Tropical cyclones and the flood
1036 hydrology of Puerto Rico, *Water Resour Res*, 41, 1–16, <https://doi.org/10.1029/2004WR003530>, 2005.

1037 Stevens, B., Giorgetta, M., Esch, M., Mauritsen, T., Crueger, T., Rast, S., Salzmann, M., Schmidt, H., Bader, J.,
1038 Block, K., Brokopf, R., Fast, I., Kinne, S., Kornblueh, L., Lohmann, U., Pincus, R., Reichler, T., and Roeckner, E.:
1039 Atmospheric component of the MPI-M Earth System Model: ECHAM6, *J Adv Model Earth Syst*, 5, 146–172,
1040 <https://doi.org/10.1002/JAME.20015>, 2013.

1041 Storlazzi, C. D., Gingerich, S. B., Van Dongeren, A., Cheriton, O. M., Swarzenski, P. W., Quataert, E., Voss, C. I.,
1042 Field, D. W., Annamalai, H., Piniak, G. A., and McCall, R.: Most atolls will be uninhabitable by the mid-21st
1043 century because of sea-level rise exacerbating wave-driven flooding, *Sci Adv*, 4, 2018.

1044 Swain, D. L., Wing, O. E. J., Bates, P. D., Done, J. M., Johnson, K., and Cameron, D. R.: Increased flood exposure
1045 due to climate change and population growth in the United States, *Earths Future*, 8,
1046 <https://doi.org/10.1029/2020ef001778>, 2020.

1047 Tan, J., Petersen, W. A., Kirstetter, P. E., and Tian, Y.: Performance of IMERG as a Function of Spatiotemporal
1048 Scale, *J Hydrometeorol*, 18, 307, <https://doi.org/10.1175/JHM-D-16-0174.1>, 2017.

1049 Tanaka, T., Kiyohara, K., and Tachikawa, Y.: Comparison of fluvial and pluvial flood risk curves in urban cities
1050 derived from a large ensemble climate simulation dataset: A case study in Nagoya, Japan, *J Hydrol (Amst)*, 584,
1051 <https://doi.org/10.1016/j.jhydrol.2020.124706>, 2020.

1052 Tang, G., Behrangi, A., Long, D., Li, C., and Hong, Y.: Accounting for spatiotemporal errors of gauges: A critical
1053 step to evaluate gridded precipitation products, *J Hydrol (Amst)*, 559, 294–306,
1054 <https://doi.org/10.1016/J.JHYDROL.2018.02.057>, 2018.

1055 Tatem, A. J.: WorldPop, open data for spatial demography, <https://doi.org/10.1038/sdata.2017.4>, 31 January 2017.

1056 Thomas, A., Pringle, P., Pflleiderer, P., and Schleussner, C.-F.: *Tropical Cyclones: Impacts, the link to Climate*
1057 *Change and Adaptation*, New York, 2017.

1058 Thomas, A., Shooya, O., Rokitzki, M., Bertrand, M., and Lissner, T.: Climate change adaptation planning in
1059 practice: insights from the Caribbean, *Reg Environ Change*, 19, 2013–2025, [https://doi.org/10.1007/s10113-019-](https://doi.org/10.1007/s10113-019-01540-5)
1060 [01540-5](https://doi.org/10.1007/s10113-019-01540-5), 2019.

1061 Thomas, A., Baptiste, A. K., Baptiste, A., Martyr-Koller, R., Pringle, P., and Rhiney, K.: Climate Change and Small
1062 Island Developing States, *Annu Rev Environ Resour*, 45, <https://doi.org/10.1146/annurev-environ-012320-083355>,
1063 2020.

1064 Tian, F., Hou, S., Yang, L., Hu, H., and Hou, A.: How Does the Evaluation of the GPM IMERG Rainfall Product
1065 Depend on Gauge Density and Rainfall Intensity?, *J Hydrometeorol*, 19, 339–349, [https://doi.org/10.1175/JHM-D-](https://doi.org/10.1175/JHM-D-17-0161.1)
1066 [17-0161.1](https://doi.org/10.1175/JHM-D-17-0161.1), 2018.

1067 Tiecke, T. G., Liu, X., Zhang, A., Gros, A., Li, N., Yetman, G., Kilic, T., Murray, S., Blankespoor, B., Prydz, E. B.,
1068 and Dang, H.-A. H.: Mapping the world population one building at a time, Washington D.C., 2017.

1069 Towe, V., Petrun Sayers, E., Chan, E., Kim, A., Tom, A., Chan, W., Marquis, J., Robbins, M., Saum-Manning, L.,
1070 Weden, M., and Payne, L.: Community Planning and Capacity Building in Puerto Rico After Hurricane Maria:
1071 Predisaster Conditions, Hurricane Damage, and Courses of Action, RAND Corporation, Santa Monica,
1072 <https://doi.org/10.7249/RR2598>, 2020.

1073 Tuholske, C., Gaughan, A. E., Sorichetta, A., de Sherbinin, A., Bucherie, A., Hultquist, C., Stevens, F.,
1074 Kruczkiewicz, A., Huyck, C., and Yetman, G.: Implications for Tracking SDG Indicator Metrics with Gridded
1075 Population Data, *Sustainability*, 13, 7329, <https://doi.org/10.3390/su13137329>, 2021.

1076 Uhe, P. F., Mitchell, D. M., Bates, P. D., Sampson, C. C., Smith, A. M., and Islam, A. S.: Enhanced flood risk with
1077 1.5 °C global warming in the Ganges–Brahmaputra–Meghna basin, *Environmental Research Letters*, 14, 074031,
1078 <https://doi.org/10.1088/1748-9326/ab10ee>, 2019.

1079 United Nations Framework Convention on Climate Change: Adoption of the Paris Agreement, Paris, 2015.

1080 United Nations Office for Disaster Risk Reduction: Global Assessment Report on Disaster Risk Reduction (5th ed.),
1081 Geneva, 2019.

1082 Terminology: <https://www.unisdr.org/we/inform/terminology>, last access: 28 October 2019.

1083 United States Geological Survey: Commonwealth of Puerto Rico QL2 Lidar Report Produced for U.S. Geological
1084 Survey, Tampa, 2017.

1085 MRMS Operational Product Viewer: https://mrms.nssl.noaa.gov/qvs/product_viewer/, last access: 22 November
1086 2023.

1087 Villarini, G., Smith, J. A., Baeck, M. L., Marchok, T., and Vecchi, G. A.: Characterization of rainfall distribution
1088 and flooding associated with U.S. landfalling tropical cyclones: Analyses of Hurricanes Frances, Ivan, and Jeanne
1089 (2004), *Journal of Geophysical Research: Atmospheres*, 116, 23116, <https://doi.org/10.1029/2011JD016175>, 2011.

1090 Vosper, E. L., Mitchell, D., and Emanuel, K.: Extreme Hurricane Rainfall affecting the Caribbean mitigated by the
1091 Paris Agreement Goals, *Environmental Research Letters*, 15, <https://doi.org/10.1088/1748-9326/ab9794>, 2020.

1092 Wehner, M. and Sampson, C.: Attributable human-induced changes in the magnitude of flooding in the Houston,
1093 Texas region during Hurricane Harvey, *Clim Change*, 166, 20, <https://doi.org/10.1007/s10584-021-03114-z>, 2021.

1094 Wehner, M. F., Reed, K. A., Li, F., Prabhat, Bacmeister, J., Chen, C. T., Paciorek, C., Gleckler, P. J., Sperber, K. R.,
1095 Collins, W. D., Gettelman, A., and Jablonowski, C.: The effect of horizontal resolution on simulation quality in the
1096 Community Atmospheric Model, CAM5.1, *J Adv Model Earth Syst*, 6, 980–997,
1097 <https://doi.org/10.1002/2013MS000276>, 2014.

1098 Williams, G. P.: Bank-full discharge of rivers, *Water Resour Res*, 14, 1141–1154,
1099 <https://doi.org/10.1029/WR014I006P01141>, 1978.

1100 Willison, C. E., Singer, P. M., Creary, M. S., and Greer, S. L.: Quantifying inequities in US federal response to
1101 hurricane disaster in Texas and Florida compared with Puerto Rico, *BMJ Glob Health*, 4,
1102 <https://doi.org/10.1136/BMJGH-2018-001191>, 2019.

1103 Wing, O. E. J., Bates, P. D., Sampson, C. C., Smith, A. M., Johnson, K. A., and Erickson, T. A.: Validation of a 30
1104 m resolution flood hazard model of the conterminous United States, *Water Resour Res*, 53, 7968–7986,
1105 <https://doi.org/10.1002/2017WR020917>, 2017.

1106 Wing, O. E. J., Bates, P. D., Smith, A. M., Sampson, C. C., Johnson, K. A., Fargione, Joseph., and Morefield,
1107 Philip.: Estimates of present and future flood risk in the conterminous United States, *Environmental Research*
1108 *Letters*, 13, <https://doi.org/10.1088/1748-9326/aaac65>, 2018.

1109 Wing, O. E. J., Sampson, C. C., Bates, P. D., Quinn, N., Smith, A. M., and Neal, J. C.: A flood inundation forecast
1110 of Hurricane Harvey using a continental-scale 2D hydrodynamic model, *J Hydrol (Amst)*, 4,
1111 <https://doi.org/10.1016/j.hydroa.2019.100039>, 2019.

1112 Wing, O. E. J., Smith, A. M., Marston, M. L., Porter, J. R., Amodeo, M. F., Sampson, C. C., and Bates, P. D.:
1113 Simulating historical flood events at the continental scale: observational validation of a large-scale hydrodynamic
1114 model, *Natural Hazards and Earth System Sciences*, 21, 559–575, <https://doi.org/10.5194/nhess-21-559-2021>, 2021.

1115 Wolman, M. G. and Miller, J. P.: Magnitude and Frequency of Forces in Geomorphic Processes, *J Geol*, 68, 54–74,
1116 1960.

1117 World Bank: Flood Hazards: Methodology Book, CHARIM: Caribbean Handbook on Disaster Risk Management,
1118 2015.

1119 World Meteorological Organization: State of the Global Climate 2021: WMO Provisional Report, Geneva, 2021.

1120 Yamazaki, D., Ikeshima, D., Tawatari, R., Yamaguchi, T., O’Loughlin, F., Neal, J. C., Sampson, C. C., Kanae, S.,
1121 and Bates, P. D.: A high-accuracy map of global terrain elevations, *Geophys Res Lett*, 44, 5844–5853,
1122 <https://doi.org/10.1002/2017GL072874>, 2017.

1123 Yamazaki, D., Ikeshima, D., Sosa, J., Bates, P. D., Allen, G. H., and Pavelsky, T. M.: MERIT Hydro: A High-
1124 Resolution Global Hydrography Map Based on Latest Topography Dataset, *Water Resour Res*, 55, 5053–5073,
1125 <https://doi.org/10.1029/2019WR024873>, 2019.

1126 Yu, C., Hu, D., Di, Y., and Wang, Y.: Performance evaluation of IMERG precipitation products during typhoon
1127 Lekima (2019), *J Hydrol (Amst)*, 597, 126307, <https://doi.org/10.1016/J.JHYDROL.2021.126307>, 2021.

1128 Zhou, G., Sun, Z., and Fu, S.: An efficient variant of the Priority-Flood algorithm for filling depressions in raster
1129 digital elevation models, *Comput Geosci*, 90, 87–96, <https://doi.org/10.1016/j.cageo.2016.02.021>, 2016.

1130 Zhu, L., Quiring, S. M., and Emanuel, K. A.: Estimating tropical cyclone precipitation risk in Texas, *Geophys Res*
1131 *Lett*, 40, 6225–6230, <https://doi.org/10.1002/2013GL058284>, 2013.

1132

1133

1134